J. Zhang, D. Ye, J.D. Biggs, Z. Sun
Finite-Time Relative Orbit-Attitude Tracking Control for Multi-Spacecraft with Collision Avoidance and Changing Network Topologies
Advances in Space Research, Vol. 63, N. 3, 2019, p. 1161-1175
doi:10.1016/j.asr.2018.10.037

Finite-time relative orbit-attitude tracking control for multi-spacecraft with collision avoidance and changing network topologies

Jianqiao Zhang[a], Dong Ye[a,*], James D. Biggs[b], Zhaowei Sun[a]

[a]*Research Center of Satellite Technology, Harbin Institute of Technology, Harbin, 150001, P.R. China.*
[b]*Department of Aerospace Science and Technology, Politecnico di Milano, Milan, 20156, Italy.*

Abstract

This paper addresses the relative position tracking and attitude synchronization control problem for spacecraft formation flying (SFF). Based on the derived relative coupled six-degree-of-freedom dynamics, a robust adaptive finite-time fast terminal sliding mode controller is proposed to achieve the desired formation in the presence of model uncertainties and external disturbances. It is shown that the designed controller is effective for changing information exchange topology making it robust to node failure. Then, the artificial potential function method is employed to generate collision avoidance schemes to modify the controller such that inter-agent collision avoidance can be ensured during the formation maneuver, which is critical for practical missions. The stability of the overall closed-loop system is proved by using Lyapunov theory. Finally, numerical examples for a given SFF scenario are presented to illustrate the performance of the controller.

Keywords: Relative position tracking and attitude synchronization; Spacecraft formation flying; Finite-time fast terminal sliding mode controller; Changing topology; Collision avoidance.

1. Introduction

Spacecraft formation flying (SFF) is a technology using multiple simpler, less-expensive, and cooperative spacecraft that can realize the functionality of large complex spacecraft [1, 2]. Furthermore, they are more flexible, responsive and robust as their formation and numbers during a mission can be adjusted [3]. These benefits could significantly enhance the possibility of new mission applications such as autonomous rendezvous and docking, interferometry, deep space applications and wide aperture Earth monitoring [4, 5]. However, these applications also require high precision control. To satisfy the control requirement of future missions, the translational and rotational motion should be considered in a coupled six-degree-of-freedom (6-DOF) framework.

For a practical space mission, a spacecraft tracks its desired states under external disturbances, and mass and inertia uncertainties due to fuel consumption and moving parts [6]. The existence of such uncertainties makes the dynamics far more complex with time-varying parameters and highly nonlinear terms[7]. Advanced robust nonlinear control approaches have been applied to improve the tracking performance of a class of complex nonlinear systems with uncertainties such as finite frequency H_∞ control for underactuated quadrotors in [8], adaptive fuzzy tracking control for nonlinear systems in [9, 10], anti-saturation robust dynamic surface control for hypersonic vehicles in [11], and also spacecraft tracking control. Developing tracking controls for spacecraft with coupled orbit-attitude dynamics has attracted considerable interest in the literature, and several robust nonlinear control theories have been developed in response, such as optimal open-loop formation reconfiguration control [12], adaptive sliding mode control [13, 14], backstepping control [15], and proportion-derivative (PD) control [16]. One example of a class of robust controls,

*Corresponding author
Email addresses: zhangjianqiao@hit.edu.cn (Jianqiao Zhang), yed@hit.edu.cn (Dong Ye), jamesdouglas.biggs@polimi.it (James D. Biggs), sunzhaowei@hit.edu.cn (Zhaowei Sun)

due to their simplicity of implementation, fast response, and good transient performance, are sliding model controls [17], which have been applied effectively in 6-DOF SFF control in [1, 18]. In [18], a sliding mode controller was designed such that each follower would track its desired states with respect to a virtual leader to achieve the desired formation. Although the controller is robust against disturbances and feasible for SFF configuration control, convergence to the desired formation is achieved in infinite time. For real-time space missions, it is critical to guarantee convergence in a realistic finite-time [19]. Moreover, finite-time stability yields a better disturbance rejection than asymptotic or exponential stability[20]. In [1], a terminal sliding mode controller was proposed to guarantee the tracking errors of the follower converge to zero in finite-time. However, this terminal sliding mode control can only provide a fast local convergence. In recent years, fast terminal sliding mode controller (FTSMC) has been developed, for it maintains fast convergence, in finite-time, globally. It has been applied successfully in SFF attitude coordination control [4], spacecraft attitude fault-tolerant control [19], spacecraft attitude tracking control [21], SFF orbit synchronization control [22], 6-DOF spacecraft tracking control [13, 23], and spacecraft hovering control over an asteroid [24].

In the existing literature, most of the 6-DOF SFF control designs assume a leader-follower architecture, such as [1, 14]. This type of control is centralized, whereby increasing the number of followers, the leader controller structure becomes more complicated, and the loss of leader will result in mission failure [25]. In contrast, a decentralized controller is generated according to each follower's desired states, which is superior in terms of robustness and reliability [26]. The decentralized virtual structure method, where each follower's tracking errors are measured with respect to a virtual leader, has been used to solve the control problem of SFF involving a mass of spacecraft in [5, 18, 25]. For a 6-DOF SFF, besides the requirement of absolute attitude and position tracking, it also requires the followers to maintain relative attitudes and an accurate geometric configuration. However, information exchange among followers is neglected in the control design in [5]. To overcome this modeling deficiency, in [18], the 6-DOF dynamics were developed in a common reference frame allowing information exchange among agents, and the decentralized control problem for SFF was investigated under undirected fixed topology. On the assumption of fixed topology, many results have been obtained to solve the decentralized relative attitude/position control problem for SFF. For example, Zou et al. [4, 26] proposed decentralized attitude controllers to guarantee the finite time stability of the SFF under undirected topology. In [27], a relative position tracking control problem for SFF, subject to directed communication topology, was addressed using sliding mode control. However, all of these decentralized controls assume a fixed topology apriori. In practice, robustness to a time-varying topology is critical for flexibility, adaptive mission scenarios and member fault.

In this paper, the relative coupled dynamics of the SFF system are developed in a compact Euler-Lagrange formulation, where information exchange among followers in a common frame is permitted. Based on the derived model, a fast terminal sliding surface is constructed, and by choosing parameters properly the singularity in [21] can be avoided. A decentralized integrated robust adaptive controller is designed via sliding mode control, adaptive control, and the virtual structure technique to guarantee the finite-time stability of the closed-loop system. The proposed controller is shown to be robust against external disturbances. In addition, system parameters can be estimated online by using the adaptive terms. Most importantly, the controller guarantees closed-loop finite-time stability independently of the type of communication topologies.

In addition to developing a robust, flexible, decentralized control with globally fast convergence, it is imperative that collision avoidance between agents during a formation maneuver should be built into the control law [28]. To solve the collision avoidance problem and maintain some form of connectivity among agents, an artificial potential function method is usually adopted for multi-agents systems [29]. This method assumes that the agents are immersed in a virtual potential field, and when they are too close, the collision avoidance acceleration generated from the negative gradient of the potential field will work as a repulsive force to prevent the agents from colliding with each other such as, collision avoidance control for Lagrangian systems in [28] and [30], decentralized relative position control with collision avoidance for SFF in [31, 32], and also decentralized control for 6-DOF SFF in [5]. More specifically, a decentralized controller with collision avoidance was proposed in [5]. However, the relative coupled dynamics were developed in the body-fixed frame of each follower, and the main problem with this formulation is that the control does not consider the local information exchange among the followers. In addition, the control objective was only achieved in infinite time. In this paper, for every SFF member, considering the relative position information

of other spacecraft within its communication region, the artificial potential function is used to modify the finite-time controller such that each agent's safety during the formation maneuver can be guaranteed. The closed-loop system is shown to remain finite-time stable after introducing the collision avoidance terms.

In summary, the main contribution of this paper is to enhance 6-DOF controls that guarantee closed-loop stability in finite-time in the presence of disturbances to include robustness to time-varying communication topologies and collision avoidance. The paper is organized as follows: In Section 2, mathematical preliminaries and the dynamical model of the relative formation flying system are presented, and the problem is formulated in a precise context. In Section 3, the main results are given. A robust adaptive finite-time controller is developed and the stability of the closed-loop system is proved. This result is extended to the case where the collision avoidance schemes are included. Simulations are conducted in Section 4 to show the effectiveness of the proposed controllers. Finally, Section 5 concludes this paper.

2. Preliminaries and problem formulation

2.1. Notation

For the convenience of expression, we define the following notations. $\boldsymbol{I}_n \in \mathbb{R}^{n\times n}$ represents a n-by-n identity matrix, and $\mathbf{0}_{n\times m} \in \mathbb{R}^{n\times m}$ denotes a n-by-m null matrix. And for a positive definite matrix $\boldsymbol{A}$, we denote $\lambda_{\max}(\boldsymbol{A})$ and $\lambda_{\min}(\boldsymbol{A})$ as its maximum and minimum eigenvalues, respectively. For a matrix $\boldsymbol{A}$ and a vector $\boldsymbol{x}$, we use $\boldsymbol{A}_i$ or $\boldsymbol{x}_i$ $(i = 1, 2, \ldots, N)$ to represent the control parameters or the system states of spacecraft i and a subscript l is used to represent the parameters of the virtual leader, where N is the number of the followers within the formation. Given a vector $\boldsymbol{x}_i = [x_i^1, x_i^2, \ \ldots, x_i^m]^{\mathrm{T}} \in \mathbb{R}^m$ and a scalar α, we define $\mathrm{sig}^{\alpha}(\boldsymbol{x}_i) = [\ |x_i^1|^{\alpha}\mathrm{sgn}(x_i^1) \quad \ldots \quad |x_i^m|^{\alpha}\mathrm{sgn}(x_i^m)\ ]^{\mathrm{T}}$, where $\mathrm{sgn}(\cdot)$ is the standard sign function. $\|\boldsymbol{x}_i\|$ represents the Euclidean norm or its induced norm. Moreover, for a vector $\boldsymbol{x}_i = [x_i^1, x_i^2, x_i^3]^{\mathrm{T}} \in \mathbb{R}^3$, $\boldsymbol{S}(\boldsymbol{x}_i)$ stands for its cross-product operator of a skew-symmetric matrix, which is given by

$$\boldsymbol{S}(\boldsymbol{x}_i) = \begin{bmatrix} 0 & -x_i^3 & x_i^2 \\ x_i^3 & 0 & -x_i^1 \\ -x_i^2 & x_i^1 & 0 \end{bmatrix} \tag{1}$$

2.2. Mathematical model of the SFF system

In this study, we consider a SFF system including a virtual leader and a group of N rigid followers. It is desired to control the followers' translational and rotational motions to specified states including predetermined position configurations and synchronized attitudes with respect to the virtual leader, whose trajectory is a circle orbit computed offline without considering external disturbances and is known to all the formation members. Moreover, the relative states between each two followers should be guaranteed. In this subsection, based on the dynamics of a single rigid spacecraft, the relative translational and rotational dynamics of the SFF system will be derived.

In order to describe the dynamic models, three necessary coordinate frames are defined first, as shown in Fig.1: (1) The standard Earth centered inertial (ECI) frame $\mathscr{F}_I(x_I, y_I, z_I)$. (2) Body-fixed frame $\mathscr{F}_b(x_b, y_b, z_b)$. Moreover, we use $\mathscr{F}_{bl}$ to represent the body-fixed frame of the virtual leader and $\mathscr{F}_{bi}$ to represent the body-fixed frame of the ith follower. (3) Local-vertical-local-horizontal (LVLH) frame $\mathscr{F}_o(x_o, y_o, z_o)$[27]. This frame is a right-handed orthogonal system, whose origin is located in the mass center of the virtual leader and is used to investigate the relative motion of the SFF system. x axis points in the radial direction from the origin of the inertia frame to the leader, z axis is normal to the orbital plane of the leader, and y axis is found by using the right-hand rule.

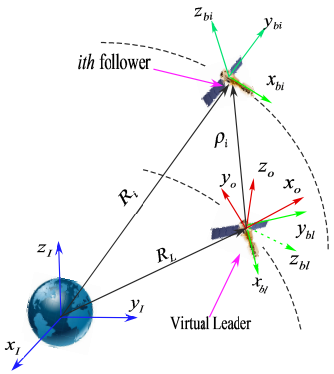

Fig. 1. Definition of the coordinate reference frames.

2.2.1. Kinematics and dynamics of a single spacecraft

Let $\boldsymbol{C} \in \mathrm{SO}(3)$ be the rotation matrix from $\mathscr{F}_b$ to $\mathscr{F}_I$, and $\boldsymbol{R} \in \mathbb{R}^3$ be the position coordinates from the origin of the ECI frame to the mass center of the spacecraft expressed in $\mathscr{F}_I$, where $\boldsymbol{C}$ is an element of SO(3), and SO(3) can be denoted by $\mathrm{SO}(3) = \{\boldsymbol{C} \in \mathbb{R}^{3\times 3} : \boldsymbol{C}^{\mathrm{T}}\boldsymbol{C} = \boldsymbol{I}_3, \det(\boldsymbol{C}) = 1\}$[33]. Then the kinematic models of a rigid spacecraft can be described by the following equations [13]

$$\begin{cases} \dot{\boldsymbol{C}} = \boldsymbol{C}\boldsymbol{S}(\boldsymbol{\omega}) \\ \dot{\boldsymbol{R}} = \boldsymbol{C}\boldsymbol{v} \end{cases} \tag{2}$$

where $\boldsymbol{\omega}$ and $\boldsymbol{v}$ are the angular velocity and translational velocity expressed in $\mathscr{F}_b$, respectively.

Let $\boldsymbol{J}$ and m be the moment of inertia matrix and the mass of the spacecraft respectively, and then the 6-DOF dynamics of the spacecraft as given in [5] can be described as:

$$\begin{cases} \boldsymbol{J}\dot{\boldsymbol{\omega}} + \boldsymbol{S}(\boldsymbol{\omega})\boldsymbol{J}\boldsymbol{\omega} = \boldsymbol{M}_{\mathrm{g}} + \boldsymbol{\tau} + \boldsymbol{d}_{\tau} \\ m\dot{\boldsymbol{v}} + m\boldsymbol{S}(\boldsymbol{\omega})\boldsymbol{v} = \boldsymbol{f}_{\mathrm{g}} + \boldsymbol{u} + \boldsymbol{d}_f \end{cases} \tag{3}$$

These equations are established in $\mathscr{F}_b$, $\boldsymbol{\tau}$ and $\boldsymbol{u}$ are the control torque and force, $\boldsymbol{d}_{\tau}$ and $\boldsymbol{d}_f$ are the disturbance torque and force, and $\boldsymbol{M}_{\mathrm{g}}$ and $\boldsymbol{f}_{\mathrm{g}}$ are gravity gradient moment and force, respectively. The translational dynamics developed here considers the Earth's oblateness to the level of J2, the second zonal harmonics, and then the specific expressions of $\boldsymbol{M}_{\mathrm{g}}$ and $\boldsymbol{f}_{\mathrm{g}}$ are given by [16]:

$$\begin{cases} \boldsymbol{M}_{\mathrm{g}} = 3\left(\frac{\mu}{\|\boldsymbol{R}\|^5}\right)\left(\boldsymbol{S}(\boldsymbol{C}^{\mathrm{T}}\boldsymbol{R})\boldsymbol{J}(\boldsymbol{C}^{\mathrm{T}}\boldsymbol{R})\right) \\ \boldsymbol{f}_{\mathrm{g}} = m(\boldsymbol{a}_g + \boldsymbol{a}_{\mathrm{J2}}),\ \boldsymbol{a}_g = -\frac{\mu\boldsymbol{C}^{\mathrm{T}}}{\|\boldsymbol{R}\|^3}\boldsymbol{R}, \\ \boldsymbol{a}_{\mathrm{J2}} = -\dfrac{3J_2\mu R_e^2\boldsymbol{C}^{\mathrm{T}}}{2\|\boldsymbol{R}\|^5}\left(\boldsymbol{D} - \dfrac{5R_z^2}{\|\boldsymbol{R}\|^2}\boldsymbol{I}_3\right)\boldsymbol{R} \end{cases} \tag{4}$$

where $\mu = 398600.44\mathrm{km}^3/\mathrm{s}^2$ is Earth's gravitational constant, $J_2 = 1.08263 \times 10^{-3}$, $R_e = 6378.14\mathrm{km}$ is the Earth's equatorial radius, $\boldsymbol{D} = \mathrm{diag}(1, 1, 3)$, and R_z is the z-axis component of $\boldsymbol{R}$.

2.2.2. Relative 6-DOF dynamics of the SFF system

In order to make information exchange among followers come true, the relative 6-DOF dynamics of the SFF system developed herein should promise that the relative attitude errors are independent of coordinate frames and the relative orbital model should be established in a common reference orbit frame. Therefore, the MRPs are used herein to represent the relative rotational dynamics, which turns out to be minimal attitude representation, and the relative translational dynamics are established in LVLH, whose center is in accordance with the virtual leader.

It should be pointed out that the virtual leader running on a particular orbit is not a real spacecraft, whose position and attitude are just used to describe the relative dynamics of the agents in formation. Thus, for the convenience of the following derivation and the implementation of the experimental tests, it is assumed that the virtual leader's attitude $\boldsymbol{C}_l$ (the rotation matrix from $\mathscr{F}_{bl}$ to $\mathscr{F}_I$) is the reference attitude of each follower, and its body fixed frame $\mathscr{F}_{bl}$ coincides perfectly with the LVLH frame $\mathscr{F}_o$.

Let $\boldsymbol{C}_i$ be the rotation matrix from $\mathscr{F}_{bi}$ to $\mathscr{F}_I$. Then the relative MRPs attitude $\boldsymbol{\sigma}_{ei}$ and relative angular velocity error $\boldsymbol{\omega}_{ei}$ of $\mathscr{F}_{bi}$ with respect to $\mathscr{F}_{bl}$ expressed in $\mathscr{F}_{bi}$ as given in [34] are

$$\boldsymbol{\sigma}_{ei} = \frac{(1-\boldsymbol{\sigma}_l^{\mathrm{T}}\boldsymbol{\sigma}_l)\boldsymbol{\sigma}_i - (1-\boldsymbol{\sigma}_i^{\mathrm{T}}\boldsymbol{\sigma}_i)\boldsymbol{\sigma}_l - 2\boldsymbol{S}(\boldsymbol{\sigma}_l)\boldsymbol{\sigma}_i}{1+\boldsymbol{\sigma}_l^{\mathrm{T}}\boldsymbol{\sigma}_l\boldsymbol{\sigma}_i^{\mathrm{T}}\boldsymbol{\sigma}_i + 2\boldsymbol{\sigma}_l^{\mathrm{T}}\boldsymbol{\sigma}_i} \tag{5}$$

$$\boldsymbol{\omega}_{ei} = \boldsymbol{\omega}_i - \boldsymbol{C}_{ei}\boldsymbol{\omega}_l \tag{6}$$

where $\boldsymbol{C}_{ei} = \boldsymbol{C}_i^{\mathrm{T}}\boldsymbol{C}_l$ is the rotational matrix from $\mathscr{F}_{bl}$ to $\mathscr{F}_{bi}$, and $\boldsymbol{\sigma}_l = \boldsymbol{n}_l\tan(\phi_l/4)$ and $\boldsymbol{\sigma}_i = \boldsymbol{n}_i\tan(\phi_i/4)$ are the MRPs of $\mathscr{F}_{bl}$ and $\mathscr{F}_{bi}$ with respect to $\mathscr{F}_I$, respectively. $\boldsymbol{n}$ is the Euler principal axis and ϕ is the Euler rotation angle, which can be calculated by the rotational matrix $\boldsymbol{C}$ [35]. The error rotational kinematics can be expressed by

$$\dot{\boldsymbol{\sigma}}_{ei} = \boldsymbol{G}(\boldsymbol{\sigma}_{ei})\boldsymbol{\omega}_{ei} \tag{7}$$

where $\boldsymbol{G}(\boldsymbol{\sigma}_{ei}) = \frac{1}{4}[(1-\boldsymbol{\sigma}_{ei}^{\mathrm{T}}\boldsymbol{\sigma}_{ei})\boldsymbol{I}_3 + 2\boldsymbol{S}(\boldsymbol{\sigma}_{ei}) + 2\boldsymbol{\sigma}_{ei}\boldsymbol{\sigma}_{ei}^{\mathrm{T}}]$, and satisfies [36]:

$$\boldsymbol{G}^{\mathrm{T}}(\boldsymbol{\sigma})\boldsymbol{G}(\boldsymbol{\sigma}) = (\frac{1+\boldsymbol{\sigma}^{\mathrm{T}}\boldsymbol{\sigma}}{4})^2\boldsymbol{I}_3 \tag{8}$$

We can calculate $\boldsymbol{\sigma}_{ei}$ based on Eqs.(2) and (5). Then motivated by [36], taking the derivative of Eq.(7), and then substituting Eqs.(3) and (6) into the result, we can obtain the second-order derivatives of $\boldsymbol{\sigma}_{ei}$, which allows us to describe the relative rotational dynamics by a Lagrange-like formulation as

$$\boldsymbol{J}_i^*\ddot{\boldsymbol{\sigma}}_{ei} + \boldsymbol{H}_{ai}\dot{\boldsymbol{\sigma}}_{ei} + \boldsymbol{\Theta}_{ai} = \boldsymbol{P}_i^{\mathrm{T}}\boldsymbol{\tau}_i + \boldsymbol{P}_i^{\mathrm{T}}\boldsymbol{M}_{gi} + \boldsymbol{P}_i^{\mathrm{T}}\boldsymbol{d}_{\tau i} \tag{9}$$

where $\boldsymbol{P}_i = \boldsymbol{G}^{-1}(\boldsymbol{\sigma}_{ei})$, $\boldsymbol{J}_i^* = \boldsymbol{P}_i^{\mathrm{T}}\boldsymbol{J}_i\boldsymbol{P}_i$, $\boldsymbol{H}_{ai} = -\boldsymbol{J}_i^*\dot{\boldsymbol{G}}(\boldsymbol{\sigma}_{ei})\boldsymbol{P}_i - \boldsymbol{P}_i^{\mathrm{T}}\big(\boldsymbol{S}(\boldsymbol{J}_i\boldsymbol{P}_i\dot{\boldsymbol{\sigma}}_{ei}) - \boldsymbol{S}(\boldsymbol{C}_{ei}\boldsymbol{\omega}_l)\boldsymbol{J}_i\big)\boldsymbol{P}_i$, $\boldsymbol{\Theta}_{ai} = \boldsymbol{P}_i^{\mathrm{T}}\big(\boldsymbol{J}_i(\boldsymbol{S}(\boldsymbol{\omega}_{ei})\boldsymbol{C}_{ei}\boldsymbol{\omega}_l + \boldsymbol{C}_{ei}\dot{\boldsymbol{\omega}}_l) + \boldsymbol{S}(\boldsymbol{C}_{ei}\boldsymbol{\omega}_l)\boldsymbol{J}_i(\boldsymbol{C}_{ei}\boldsymbol{\omega}_l)\big)$.

Furthermore, for on-orbit spacecraft, which suffers disturbances, fuel consuming and environmental influences, it is impossible for the inertia tensor and the mass of the spacecraft to be known exactly. Consequently, we use $\boldsymbol{J}_{1i} = \boldsymbol{J}_i + \Delta\boldsymbol{J}_i$ to represent the actual inertia of a follower as in [17], where $\Delta\boldsymbol{J}_i$ is the uncertain part of the inertia. By regarding the inertia uncertainties and the external disturbances as the total disturbances of the follower, we can rewrite Eq.(9) as

$$\boldsymbol{J}_i^*\ddot{\boldsymbol{\sigma}}_{ei} + \boldsymbol{H}_{ai}\dot{\boldsymbol{\sigma}}_{ei} + \boldsymbol{\Theta}_{ai} = \boldsymbol{P}_i^{\mathrm{T}}\boldsymbol{\tau}_i + \Delta\boldsymbol{d}_{\tau i} \tag{10}$$

where $\Delta\boldsymbol{d}_{\tau i} = -\boldsymbol{P}_i^{\mathrm{T}}\big(\Delta\boldsymbol{J}_i\boldsymbol{P}_i\ddot{\boldsymbol{\sigma}}_{ei} - \Delta\boldsymbol{J}_i\boldsymbol{P}_i\dot{\boldsymbol{G}}(\boldsymbol{\sigma}_{ei})\boldsymbol{P}_i\dot{\boldsymbol{\sigma}}_{ei} - \boldsymbol{S}(\Delta\boldsymbol{J}_i\boldsymbol{P}_i\dot{\boldsymbol{\sigma}}_{ei})\boldsymbol{P}_i\dot{\boldsymbol{\sigma}}_{ei} + \boldsymbol{S}(\boldsymbol{C}_{ei}\boldsymbol{\omega}_l)\Delta\boldsymbol{J}_i\boldsymbol{P}_i\dot{\boldsymbol{\sigma}}_{ei} - \boldsymbol{M}_{gi} - \boldsymbol{d}_{\tau i} + \Delta\boldsymbol{J}_i\big(\boldsymbol{S}(\boldsymbol{\omega}_{ei})\boldsymbol{C}_{ei}\boldsymbol{\omega}_l + \boldsymbol{C}_{ei}\dot{\boldsymbol{\omega}}_l\big) + \boldsymbol{S}(\boldsymbol{C}_{ei}\boldsymbol{\omega}_l)\Delta\boldsymbol{J}_i(\boldsymbol{C}_{ei}\boldsymbol{\omega}_l)\big)$.

Let $\boldsymbol{R}_i$ and $\boldsymbol{R}_l$ denote the position vector of follower i and the virtual leader expressed in $\mathscr{F}_I$, respectively. To establish the relative translational dynamics, we define the relative position from the leader to ith follower as $\boldsymbol{\rho}_i = \boldsymbol{C}_l^{\mathrm{T}}(\boldsymbol{R}_i - \boldsymbol{R}_l) = [x_i, y_i, z_i]^{\mathrm{T}}$ and their desired relative position as $\boldsymbol{\rho}_i^d = \boldsymbol{C}_l^{\mathrm{T}}(\boldsymbol{R}_i^d - \boldsymbol{R}_l)$, both of which are represented in $\mathscr{F}_o$. Then the relative position tracking error of ith follower can be denoted by $\tilde{\boldsymbol{\rho}}_i = \boldsymbol{\rho}_i - \boldsymbol{\rho}_i^d$, and $\dot{\tilde{\boldsymbol{\rho}}}_i = \dot{\boldsymbol{\rho}}_i - \dot{\boldsymbol{\rho}}_i^d$ is its velocity. Then motivated by [27] and from Eq.(3), the relative orbital motion can be obtained as

$$m_i\ddot{\tilde{\boldsymbol{\rho}}}_i + \boldsymbol{H}_{bi}\dot{\tilde{\boldsymbol{\rho}}}_i + \boldsymbol{\Theta}_{bi} = \boldsymbol{C}_l^{\mathrm{T}}\boldsymbol{C}_i\boldsymbol{u}_i + \boldsymbol{C}_l^{\mathrm{T}}\boldsymbol{C}_i\boldsymbol{d}_{fi} \tag{11}$$

where $\boldsymbol{H}_{bi} = m_i\boldsymbol{S}(\boldsymbol{\ell})$, $\boldsymbol{\ell} = [0, 0, 2\dot{\theta}]^{\mathrm{T}}$, $\boldsymbol{\Theta}_{bi} = m_i\boldsymbol{a}_{\boldsymbol{\Theta}_{bi}}$, $\boldsymbol{a}_{\boldsymbol{\Theta}_{bi}} = \boldsymbol{a}_{\theta i} + \boldsymbol{H}_{bi}\dot{\boldsymbol{\rho}}_i^d + \ddot{\boldsymbol{\rho}}_i^d + \boldsymbol{a}_{J2l} - \boldsymbol{S}(\boldsymbol{\omega}_l)\boldsymbol{v}_l - \boldsymbol{C}_l^{\mathrm{T}}\boldsymbol{C}_i\boldsymbol{a}_{J2i} + \boldsymbol{C}_l^{\mathrm{T}}\boldsymbol{C}_i\boldsymbol{S}(\boldsymbol{\omega}_i)\boldsymbol{v}_i$, and

$$\boldsymbol{a}_{\theta i} = \begin{bmatrix} -\ddot{\theta}y_i - \dot{\theta}^2 x_i + \frac{\mu(x_i + \|\boldsymbol{R}_l\|)}{\|\boldsymbol{R}_l + \boldsymbol{C}_l\boldsymbol{\rho}_i\|^3} - \frac{\mu}{\|\boldsymbol{R}_l\|^2} \\ \ddot{\theta}x_i - \dot{\theta}^2 y_i + \frac{\mu y_i}{\|\boldsymbol{R}_l + \boldsymbol{C}_l\boldsymbol{\rho}_i\|^3} \\ \frac{\mu z_i}{\|\boldsymbol{R}_l + \boldsymbol{C}_l\boldsymbol{\rho}_i\|^3} \end{bmatrix} \tag{12}$$

where θ is the true anomaly of the leader, which satisfies $\|\boldsymbol{R}_l\| = \frac{a_l(1-e_l^2)}{1+e_l\cos\theta}$, a_l and e_l are the semi-major axis and orbital eccentricity of the leader, respectively. Let $n_l = \sqrt{\mu/a_l^3}$ denote the mean orbital angular velocity, and then $\dot{\theta}$, $\ddot{\theta}$ can be obtained by

$$\begin{cases} \dot{\theta} = \dfrac{n_l(1 + e_l\cos\theta)^2}{(1 - e_l^2)^{\frac{3}{2}}} \\ \ddot{\theta} = \dfrac{-2n_l^2(1 + e_l\cos\theta)^3 e_l\sin\theta}{(1 - e_l^2)^3} \end{cases} \tag{13}$$

Denote the mass uncertainty part be Δm_i, and then similar as Eq.(10), we can rewrite the relative translational dynamics as

$$m_i\ddot{\widetilde{\boldsymbol{\rho}}}_i + \boldsymbol{H}_{bi}\dot{\widetilde{\boldsymbol{\rho}}}_i + \boldsymbol{\Theta}_{bi} = \boldsymbol{C}_l^{\mathrm{T}}\boldsymbol{C}_i\boldsymbol{u}_i + \Delta\boldsymbol{d}_{fi} \tag{14}$$

where $\Delta\boldsymbol{d}_{fi} = \boldsymbol{C}_l^{\mathrm{T}}\boldsymbol{C}_i\boldsymbol{d}_{fi} - \Delta m_i\big(\boldsymbol{S}(\boldsymbol{\ell})\dot{\boldsymbol{\rho}}_i + \ddot{\boldsymbol{\rho}}_i + \boldsymbol{a}_{\theta i} + \boldsymbol{a}_{J2l} - \boldsymbol{S}(\boldsymbol{\omega}_l)\boldsymbol{v}_l - \boldsymbol{C}_l^{\mathrm{T}}\boldsymbol{C}_i\boldsymbol{a}_{J2i} + \boldsymbol{C}_l^{\mathrm{T}}\boldsymbol{C}_i\boldsymbol{S}(\boldsymbol{\omega}_i)\boldsymbol{v}_i\big)$.

In combination with (10), (14) and defining $\boldsymbol{\xi}_i = [\boldsymbol{\sigma}_{ei}^{\mathrm{T}}, \widetilde{\boldsymbol{\rho}}_i^{\mathrm{T}}]^{\mathrm{T}}$, we can describe the relative 6-DOF dynamics in a united framework as

$$\boldsymbol{M}_i\ddot{\boldsymbol{\xi}}_i + \boldsymbol{H}_i\dot{\boldsymbol{\xi}}_i + \boldsymbol{\Theta}_i = \mathscr{B}_i\boldsymbol{\Gamma}_{\mathrm{ci}} + \Delta\boldsymbol{d}_i \tag{15}$$

where $\boldsymbol{M}_i = \mathrm{diag}(\boldsymbol{J}_i^*, m\boldsymbol{I}_3)$, $\boldsymbol{H}_i = \mathrm{diag}(\boldsymbol{H}_{ai}, \boldsymbol{H}_{bi})$, $\boldsymbol{\Theta}_i = \mathrm{diag}(\boldsymbol{\Theta}_{ai}, \boldsymbol{\Theta}_{bi})$, $\mathscr{B}_i = \mathrm{diag}(\boldsymbol{P}_i^{\mathrm{T}}, \boldsymbol{C}_l^{\mathrm{T}}\boldsymbol{C}_i)$, $\boldsymbol{\Gamma}_{\mathrm{ci}} = [\boldsymbol{\tau}_i^{\mathrm{T}}, \boldsymbol{u}_i^{\mathrm{T}}]^{\mathrm{T}}$, $\Delta\boldsymbol{d}_i = [\Delta\boldsymbol{d}_{\tau i}^{\mathrm{T}}, \Delta\boldsymbol{d}_{fi}^{\mathrm{T}}]^{\mathrm{T}}$.

This model is a standard Euler-Lagrange formulation and has the following well known structural features, similar as usual Euler-Lagrange systems [37]:

Property 1. *(P1) $\boldsymbol{M}_i$ is a symmetric positive definite matrix and it is bounded, which means that there exist two positive constants λ_1, λ_2 and $\lambda_1 \le \lambda_2$ such that $\lambda_1\|\boldsymbol{x}\|^2 \le \boldsymbol{x}^{\mathrm{T}}\boldsymbol{M}_i(\boldsymbol{\xi}_i)\boldsymbol{x} \le \lambda_2\|\boldsymbol{x}\|^2$ holds for all $\boldsymbol{x}, \boldsymbol{\xi}_i \in \mathbb{R}^6$.*

Property 2. *(P2) $\dot{\boldsymbol{M}}_i - 2\boldsymbol{H}_i$ is a skew-symmetric matrix, which satisfies $\boldsymbol{x}^{\mathrm{T}}(\dot{\boldsymbol{M}}_i - 2\boldsymbol{H}_i)\boldsymbol{x} = 0$ for all $\boldsymbol{x} \in \mathbb{R}^6$.*

Remark 1. Considering the structured and unstructured uncertainties, Eq. (15) forms the relative 6-DOF dynamics of the SFF system investigated in this research, in which the relative translational and rotational motion are described in a united framework with their dynamical couplings included in $\boldsymbol{\Theta}_i$. The coupled effect of the angular velocity on translational dynamics is considered, and as such provides a more realistic model than the current state of the art used in [18]. The relative translational dynamics introduced herein has high accuracy in any eccentric orbits when the distances among formation members are not very far. Moreover, as discussed in [36], it should be noted that the relative attitude error will be nonsingular and bounded by switching between the MRPs $\boldsymbol{\sigma}$ and its corresponding shadow $\boldsymbol{\sigma}^s = -\boldsymbol{\sigma}/(\boldsymbol{\sigma}^{\mathrm{T}}\boldsymbol{\sigma})$. Furthermore, by designing an appropriate controller $\boldsymbol{\Gamma}_{\mathrm{ci}}$, the relative orbit and attitude tracking control can be realized with high accuracy simultaneously to satisfy the requirements of some spacecraft proximity operations, which is superior than describing the 6-DOF model independently without considering the dynamical coupling.

2.3. Assumptions and lemmas

In space applications, the environmental disturbances can be characterized into gravitational forces, solar radiation pressure, air drag, gravity gradient perturbations and magnetic dipole effects. All of these, although possibly not precisely determined, can be characterized by an upper-bound on the disturbance torque and force. In addition, the uncertainties in mass and inertia properties due to fuel consumption and moving parts are naturally bounded. Furthermore, for close spacecraft operation, the relative tracking error $\boldsymbol{\xi}_i$ and its first two derivatives are bounded. Thus it is reasonable to give the following assumption:

Assumption 1. The disturbance $\Delta \boldsymbol{d}_i$ is unknown but bounded such that $|\Delta \boldsymbol{d}_i^k| \leq \delta_i^k, k = 1, 2, \cdots 6$, where $\boldsymbol{\delta}_i \in \mathbb{R}^{6\times 1}$ is a positive constant vector.

In order to facilitate the stability analysis of the control laws, the following useful lemmas are presented.

Lemma 1. *([19]) Suppose that there exists a continuous positive definite function $V(t) : \mathbb{R}^n \to \mathbb{R}$, which satisfies the following differential inequality:*

$$\dot{V}(t) + \varpi_1 V(t) + \varpi_2 V^{\varpi}(t) \leq 0, \forall t > t_0 \tag{16}$$

where $\varpi_1 > 0, \varpi_2 > 0$, and $0 < \varpi < 1$. Then $V(t)$ can converge to the equilibrium in finite time t_f, where

$$t_f \leq t_0 + \frac{1}{\varpi_1(1-\varpi)} \ln \frac{\varpi_1 V^{1-\varpi}(t_0) + \varpi_2}{\varpi_2} \tag{17}$$

Definition 1. ([38]) Consider the perturbed system $\dot{\boldsymbol{x}} = \boldsymbol{f}(t, \boldsymbol{x}) + \boldsymbol{g}(t, \boldsymbol{x})$, where $\dot{\boldsymbol{x}} = \boldsymbol{f}$ is the nominal system and $\boldsymbol{g}$ is its perturbation. If $\boldsymbol{g}(t, \boldsymbol{0}) = \boldsymbol{0}$, which means that $\boldsymbol{g}$ vanishes at the equilibrium $\boldsymbol{x} = \boldsymbol{0}$, then $\boldsymbol{g}$ is defined as the vanishing perturbation of the perturbed system.

Lemma 2. *([31]) Let $\boldsymbol{x} = \boldsymbol{0}$ be a finite-time stable equilibrium of the nominal system $\dot{\boldsymbol{x}} = \boldsymbol{f}(t, \boldsymbol{x})$. If the Lyapunov function of the nominal system $V(t, \boldsymbol{x})$ satisfies the following inequalities with some positive scalars $\beta_k, (k = 1, \cdots, 5)$ and $0 < \gamma < 1$*

$$\begin{aligned} &\beta_1 \|\boldsymbol{x}\|^2 \leq V(t, \boldsymbol{x}) \leq \beta_2 \|\boldsymbol{x}\|^2 \\ &\frac{\partial V}{\partial t} + \frac{\partial V}{\partial \boldsymbol{x}} \boldsymbol{f}(t, \boldsymbol{x}) \leq -\beta_3 \|\boldsymbol{x}\|^2 - \beta_4 \|\boldsymbol{x}\|^{2\gamma} \\ &\| \frac{\partial V}{\partial \boldsymbol{x}} \| \leq \beta_5 \|\boldsymbol{x}\| \end{aligned} \tag{18}$$

and the vanishing perturbation $\boldsymbol{g}(t, \boldsymbol{x})$ is assumed to satisfy

$$\|\boldsymbol{g}(t, \boldsymbol{x})\| \leq \kappa \|\boldsymbol{x}\|, \text{and } \kappa < \beta_3/\beta_5 \tag{19}$$

then $\boldsymbol{x} = \boldsymbol{0}$ is a finite-time stable equilibrium of the perturbed system $\dot{\boldsymbol{x}} = \boldsymbol{f}(t, \boldsymbol{x}) + \boldsymbol{g}(t, \boldsymbol{x})$. Moreover, if all the above inequalities hold globally, then the origin is a global finite-time stable equilibrium of the system.

2.4. Problem statement

In this study, we investigate the relative motion control problem of a SFF system. The control objective herein can be stated as follows: Considering the relative 6-DOF dynamics governed by Eq. (15) with the above reasonable assumption holding, our purpose is to design suitable control schemes such that the rotational and translational motion of each follower can converge to their desired states with respect to the virtual leader in the presence of model uncertainties and external disturbances in finite time. Moreover, in order to make the SFF system perform as a whole rather than several individuals, and enhance formation-keeping and attitude consensus performance, coordination terms among the followers are considered such

that the desired relative states between each two followers can be promised. That is to say $\lim_{t\to t_f}\boldsymbol{\xi}_i = \lim_{t\to t_f}\dot{\boldsymbol{\xi}}_i = 0$, $\lim_{t\to t_f}\boldsymbol{\rho}_{ij} - \boldsymbol{\rho}_{ij}^d = \lim_{t\to t_f}\dot{\boldsymbol{\rho}}_{ij} - \dot{\boldsymbol{\rho}}_{ij}^d = 0$, and $\lim_{t\to t_f}\boldsymbol{\sigma}_{ij} = \lim_{t\to t_f}\dot{\boldsymbol{\sigma}}_{ij} = 0$. The controller should be effective with no assumption on the information exchange graph. Furthermore, collision avoidance problem should be addressed during the formation maneuver.

3. Controller design and stability analysis

The main results will be presented in this section. Based on the existing results on FTSMC, a class of robust adaptive control laws are proposed to achieve the control objective. Meanwhile, the finite-time stability of the developed controllers will be given by employing Lyapunov methods.

3.1. Robust adaptive finite-time controller synthesis

To guarantee the finite-time stability of the SFF system, a fast terminal sliding surface is first designed such that once the system states arriving on it, then they can converge to the equilibrium in finite time. The form of the sliding surface is defined as

$$\boldsymbol{S}_i = \dot{\boldsymbol{\xi}}_i + \boldsymbol{\vartheta}_{1i}\boldsymbol{\xi}_i + \boldsymbol{\vartheta}_{2i}\mathrm{sig}^{\alpha}(\boldsymbol{\xi}_i) \tag{20}$$

where $\boldsymbol{\vartheta}_{1i}, \boldsymbol{\vartheta}_{2i} \in \mathbb{R}^{6\times 6}$ are positive definite diagonal matrices, and $0.5 < \alpha < 1$. Denoting $\boldsymbol{q}_i = \boldsymbol{\vartheta}_{1i}\boldsymbol{\xi}_i + \boldsymbol{\vartheta}_{2i}\mathrm{sig}^{\alpha}(\boldsymbol{\xi}_i)$ and $\dot{\boldsymbol{q}}_i = \boldsymbol{\vartheta}_{1i}\dot{\boldsymbol{\xi}}_i + \alpha\boldsymbol{\vartheta}_{2i}\mathrm{diag}(\mathrm{sig}^{\alpha-1}(\boldsymbol{\xi}_i))\dot{\boldsymbol{\xi}}_i$, and combining Eq. (15) and Eq. (20) yields

$$\boldsymbol{M}_i\dot{\boldsymbol{S}}_i + \boldsymbol{H}_i\boldsymbol{S}_i = \boldsymbol{M}_i\dot{\boldsymbol{q}}_i + \boldsymbol{H}_i\boldsymbol{q}_i - \boldsymbol{\Theta}_i + \mathscr{B}_i\boldsymbol{\Gamma}_{\mathrm{ci}} + \Delta\boldsymbol{d}_i \tag{21}$$

Since for on-orbit spacecraft, the inertia and mass of the spacecraft are usually unknown, to estimate these values, motivated by [14], a linear operator $\boldsymbol{L}$ acting on a vector $\boldsymbol{y} = [y_1, y_2, y_3]^{\mathrm{T}} \in \mathbb{R}^3$ is defined first as follows:

$$\boldsymbol{L}(\boldsymbol{y}) = \begin{bmatrix} y_1 & 0 & 0 & 0 & y_3 & y_2 \\ 0 & y_2 & 0 & y_3 & 0 & y_1 \\ 0 & 0 & y_3 & y_2 & y_1 & 0 \end{bmatrix} \tag{22}$$

Then we have $\boldsymbol{J}_i\boldsymbol{y} = \boldsymbol{L}(\boldsymbol{y})\boldsymbol{\nu}(\boldsymbol{J}_i)$, $\boldsymbol{\nu}(\boldsymbol{J}_i) = [(\boldsymbol{J}_i)_{11}, (\boldsymbol{J}_i)_{22}, (\boldsymbol{J}_i)_{33}, (\boldsymbol{J}_i)_{23}, (\boldsymbol{J}_i)_{13}, (\boldsymbol{J}_i)_{12}]^{\mathrm{T}} \in \mathbb{R}^6$. Thus, (21) can be rewritten as

$$\boldsymbol{M}_i\dot{\boldsymbol{S}}_i + \boldsymbol{H}_i\boldsymbol{S}_i = \boldsymbol{Y}_i(\boldsymbol{\xi}_i, \dot{\boldsymbol{\xi}}_i)\boldsymbol{\nu}(\boldsymbol{\Xi}_i) + \mathscr{B}_i\boldsymbol{\Gamma}_{\mathrm{ci}} + \Delta\boldsymbol{d}_i \tag{23}$$

where $\boldsymbol{\nu}(\boldsymbol{\Xi}_i) = [(\boldsymbol{J}_i)_{11}, (\boldsymbol{J}_i)_{22}, (\boldsymbol{J}_i)_{33}, (\boldsymbol{J}_i)_{23}, (\boldsymbol{J}_i)_{13}, (\boldsymbol{J}_i)_{12}, m_i]^{\mathrm{T}}$, and $\boldsymbol{Y}_i(\boldsymbol{\xi}_i, \dot{\boldsymbol{\xi}}_i) = \mathrm{diag}\big(\boldsymbol{Y}_i(\boldsymbol{\sigma}_{ei}, \dot{\boldsymbol{\sigma}}_{ei}), \boldsymbol{Y}_i(\widetilde{\boldsymbol{\rho}}_i, \dot{\widetilde{\boldsymbol{\rho}}}_i)\big) \in \mathbb{R}^{6\times 7}$. $\boldsymbol{Y}_i(\boldsymbol{\sigma}_{ei}, \dot{\boldsymbol{\sigma}}_{ei}) \in \mathbb{R}^{3\times 6}$ and $\boldsymbol{Y}_i(\widetilde{\boldsymbol{\rho}}_i, \dot{\widetilde{\boldsymbol{\rho}}}_i) \in \mathbb{R}^{3\times 1}$ are defined explicitly with the following expressions:

$$\begin{cases} \boldsymbol{Y}_i(\boldsymbol{\sigma}_{ei}, \dot{\boldsymbol{\sigma}}_{ei}) = \boldsymbol{P}_i^{\mathrm{T}}\Big(\boldsymbol{L}(\boldsymbol{P}_i[\dot{\boldsymbol{q}}_i]_1) - \boldsymbol{L}\big(\boldsymbol{P}_i\dot{\boldsymbol{G}}(\boldsymbol{\sigma}_{ei})\boldsymbol{P}_i[\boldsymbol{q}_i]_1\big) + \boldsymbol{S}(\boldsymbol{C}_{ei}\boldsymbol{\omega}_l)\boldsymbol{L}(\boldsymbol{C}_{ei}\boldsymbol{\omega}_l) \\ \qquad + \boldsymbol{S}(\boldsymbol{P}_i[\boldsymbol{q}_i]_1)\boldsymbol{L}(\boldsymbol{P}_i\dot{\boldsymbol{\sigma}}_{ei}) - \boldsymbol{L}\big(\boldsymbol{S}(\boldsymbol{\omega}_{ei})\boldsymbol{C}_{ei}\boldsymbol{\omega}_l + \boldsymbol{C}_{ei}\dot{\boldsymbol{\omega}}_l\big)\Big), \\ \boldsymbol{Y}_i(\widetilde{\boldsymbol{\rho}}_i, \dot{\widetilde{\boldsymbol{\rho}}}_i) = [\dot{\boldsymbol{q}}_i]_2 + \boldsymbol{S}(\boldsymbol{\ell})[\boldsymbol{q}_i]_2 - \boldsymbol{a}_{\boldsymbol{\Theta}_{bi}} \end{cases}$$

where $[\boldsymbol{q}_i]_1 = [\boldsymbol{q}_i^1, \boldsymbol{q}_i^2, \boldsymbol{q}_i^3]^{\mathrm{T}}$ and $[\boldsymbol{q}_i]_2 = [\boldsymbol{q}_i^4, \boldsymbol{q}_i^5, \boldsymbol{q}_i^6]^{\mathrm{T}}$. To this end, the first main result of this study is presented as follows:

Theorem 1. *For the SFF system governed by (23), Assumption 1 is satisfied and the control scheme is designed as:*

$$\boldsymbol{\Gamma}_{\mathrm{ci}} = \mathscr{B}_i^{-1}\Big(-\boldsymbol{Y}_i(\boldsymbol{\xi}_i, \dot{\boldsymbol{\xi}}_i)\hat{\boldsymbol{\nu}}(\boldsymbol{\Xi}_i) - \boldsymbol{K}_{1i}\boldsymbol{S}_i - \boldsymbol{K}_{2i}\mathrm{sgn}(\boldsymbol{S}_i) - \sum_{j=1}^{N}(\boldsymbol{k}_{ij}\boldsymbol{S}_i - o_{ij}\boldsymbol{k}_j\boldsymbol{S}_j)\Big) \tag{24}$$

where $\boldsymbol{K}_{1i}, \boldsymbol{K}_{2i}, \boldsymbol{k}_{ij}, \boldsymbol{k}_j \in \mathbb{R}^{6\times 6}$ *are all positive definite diagonal matrices.* o_{ij} *is a time-varying binary number, if there is interconnection between spacecraft* i *and* j, $o_{ij} = 1$, *otherwise* $o_{ij} = 0$. $\hat{\boldsymbol{\nu}}(\boldsymbol{\Xi}_i)$ *is the estimation of* $\boldsymbol{\nu}(\boldsymbol{\Xi}_i)$, *which is updated by*

$$\dot{\hat{\boldsymbol{\nu}}}(\boldsymbol{\Xi}_i) = \boldsymbol{\Lambda}_i \boldsymbol{Y}_i^{\mathrm{T}}(\boldsymbol{\xi}_i, \dot{\boldsymbol{\xi}}_i)\boldsymbol{S}_i \tag{25}$$

where $\boldsymbol{\Lambda}_i \in \mathbb{R}^{7\times 7}$ *is a positive definite diagonal matrix. If the control parameters are designed such that* $\lambda_{\min}(\boldsymbol{k}_{ij}) > \hbar_{ij}$, $[\boldsymbol{K}_{2i}]_k > \varphi_i^k$, *where* $[\boldsymbol{K}_{2i}]_k$ *is the* k*th element on the main diagonal of* $\boldsymbol{K}_{2i}$, *and* $\hbar_{ij}(4\lambda_{\min}(\boldsymbol{k}_{ij}) - \hbar_{ij}) \geqslant o_{ij}\lambda_{\max}^2(\boldsymbol{k}_j)$, *then the finite-time stability of the closed-loop SFF system can be guaranteed.*

Proof. The proof of this theorem can be divided into the following two steps:

(1) The sliding surface $\boldsymbol{S}_i$ is finite-time stable under controller (24) with the adaptive law (25);

(2) Once the sliding surface $\boldsymbol{S}_i = \boldsymbol{0}$ has been reached, its two components $\boldsymbol{\xi}_i$ and $\dot{\boldsymbol{\xi}}_i$ will reach the origin in finite-time, independently.

To prove step 1, the following candidate Lyapunov function is considered:

$$V_1 = \sum_{i=1}^{N} V_{1i} = \sum_{i=1}^{N} \Big(\frac{1}{2}\boldsymbol{S}_i^{\mathrm{T}}\boldsymbol{M}_i\boldsymbol{S}_i + \frac{1}{2}\widetilde{\boldsymbol{\nu}}^{\mathrm{T}}(\boldsymbol{\Xi}_i)\boldsymbol{\Lambda}_i^{-1}\widetilde{\boldsymbol{\nu}}(\boldsymbol{\Xi}_i)\Big) \tag{26}$$

where $\widetilde{\boldsymbol{\nu}}(\boldsymbol{\Xi}_i) = \hat{\boldsymbol{\nu}}(\boldsymbol{\Xi}_i) - \boldsymbol{\nu}(\boldsymbol{\Xi}_i)$, and by using P1 it is obvious that V_1 is positive. Taking the time derivative of V_1 along Eq. (23), yields

$$\begin{aligned}
\dot{V}_1 &= \sum_{i=1}^{N} \Big(\boldsymbol{S}_i^{\mathrm{T}}\boldsymbol{M}_i\dot{\boldsymbol{S}}_i + \frac{1}{2}\boldsymbol{S}_i^{\mathrm{T}}\dot{\boldsymbol{M}}_i\boldsymbol{S}_i + \widetilde{\boldsymbol{\nu}}^{\mathrm{T}}(\boldsymbol{\Xi}_i)\boldsymbol{\Lambda}_i^{-1}\dot{\widetilde{\boldsymbol{\nu}}}(\boldsymbol{\Xi}_i)\Big) \\
&= \sum_{i=1}^{N} \boldsymbol{S}_i^{\mathrm{T}}\Big(-\boldsymbol{H}_i\boldsymbol{S}_i + \boldsymbol{Y}_i(\boldsymbol{\xi}_i, \dot{\boldsymbol{\xi}}_i)\boldsymbol{\nu}(\boldsymbol{\Xi}_i) + \mathscr{B}_i\boldsymbol{\Gamma}_{\mathrm{ci}} + \Delta\boldsymbol{d}_i\Big) + \frac{1}{2}\sum_{i=1}^{N}\boldsymbol{S}_i^{\mathrm{T}}\dot{\boldsymbol{M}}_i\boldsymbol{S}_i + \sum_{i=1}^{N}\widetilde{\boldsymbol{\nu}}^{\mathrm{T}}(\boldsymbol{\Xi}_i)\boldsymbol{\Lambda}_i^{-1}\dot{\widetilde{\boldsymbol{\nu}}}(\boldsymbol{\Xi}_i)
\end{aligned}$$

Using P2 that $\boldsymbol{x}^{\mathrm{T}}(\dot{\boldsymbol{M}}_i - 2\boldsymbol{H}_i)\boldsymbol{x} = 0$ and substituting Eqs. (24), (25) into it, one can obtain

$$\begin{aligned}
\dot{V}_1 &= \sum_{i=1}^{N} \boldsymbol{S}_i^{\mathrm{T}}\Big(-\boldsymbol{Y}_i(\boldsymbol{\xi}_i, \dot{\boldsymbol{\xi}}_i)\widetilde{\boldsymbol{\nu}}(\boldsymbol{\Xi}_i) - \boldsymbol{K}_{1i}\boldsymbol{S}_i - \boldsymbol{K}_{2i}\mathrm{sgn}(\boldsymbol{S}_i) - \sum_{j=1}^{N}(\boldsymbol{k}_{ij}\boldsymbol{S}_i - o_{ij}\boldsymbol{k}_j\boldsymbol{S}_j) + \boldsymbol{Y}_i(\boldsymbol{\xi}_i, \dot{\boldsymbol{\xi}}_i)\widetilde{\boldsymbol{\nu}}(\boldsymbol{\Xi}_i) + \Delta\boldsymbol{d}_i\Big) \\
&\leq -\sum_{i=1}^{N}\boldsymbol{S}_i^{\mathrm{T}}\boldsymbol{K}_{1i}\boldsymbol{S}_i - \sum_{i=1}^{N}\sum_{k=1}^{6}\Big([\boldsymbol{K}_{2i}]_k - \delta_i^k\Big)|\boldsymbol{S}_i^k| - \sum_{i=1}^{N}\sum_{j=1}^{N}\Big(\lambda_{\min}(\boldsymbol{k}_{ij})\boldsymbol{S}_i^{\mathrm{T}}\boldsymbol{S}_i - o_{ij}\boldsymbol{S}_i^{\mathrm{T}}\boldsymbol{k}_j\boldsymbol{S}_j\Big)
\end{aligned} \tag{27}$$

Note that for a SFF system, the following equation holds:

$$\sum_{i=1}^{N}\sum_{j=1}^{N}\hbar_{ij}\big(\boldsymbol{S}_i^{\mathrm{T}}\boldsymbol{S}_i - \boldsymbol{S}_j^{\mathrm{T}}\boldsymbol{S}_j\big) = 0 \tag{28}$$

where $\hbar_{ij} = \hbar_{ji} > 0$. Then adding Eq. (28) to both sides of Eq. (27), we have

$$\begin{aligned}
\dot{V}_1 &\leq -\sum_{i=1}^{N}\boldsymbol{S}_i^{\mathrm{T}}\boldsymbol{K}_{1i}\boldsymbol{S}_i - \sum_{i=1}^{N}\sum_{j=1}^{N}(\lambda_{\min}(\boldsymbol{k}_{ij}) - \hbar_{ij})\boldsymbol{S}_i^{\mathrm{T}}\boldsymbol{S}_i + \sum_{i=1}^{N}\sum_{j=1}^{N}o_{ij}\boldsymbol{S}_i^{\mathrm{T}}\boldsymbol{k}_j\boldsymbol{S}_j - \sum_{i=1}^{N}\sum_{j=1}^{N}\hbar_{ij}\boldsymbol{S}_j^{\mathrm{T}}\boldsymbol{S}_j \\
&\leq -\sum_{i=1}^{N}\boldsymbol{S}_i^{\mathrm{T}}\boldsymbol{K}_{1i}\boldsymbol{S}_i - \sum_{i=1}^{N}\sum_{j=1}^{N}\boldsymbol{\Upsilon}_{ij}^{\mathrm{T}}\boldsymbol{\Upsilon}_{ij} - \sum_{i=1}^{N}\sum_{j=1}^{N}\pounds_{ij}\boldsymbol{S}_j^{\mathrm{T}}\boldsymbol{S}_j
\end{aligned}$$

where $\boldsymbol{\Upsilon}_{ij} = \sqrt{\lambda_{\min}(\boldsymbol{k}_{ij}) - \hbar_{ij}}\boldsymbol{S}_i - \dfrac{o_{ij}\boldsymbol{k}_j}{2\sqrt{\lambda_{\min}(\boldsymbol{k}_{ij}) - \hbar_{ij}}}\boldsymbol{S}_j$, and $\pounds_{ij} = \hbar_{ij} - \dfrac{o_{ij}\lambda^2_{\max}(\boldsymbol{k}_j)}{4\lambda_{\min}(\boldsymbol{k}_{ij}) - \hbar_{ij}}$.

When $\lambda_{\min}(\boldsymbol{k}_{ij}) > \hbar_{ij}$ and $\hbar_{ij}(4\lambda_{\min}(\boldsymbol{k}_{ij}) - \hbar_{ij}) \geqslant o_{ij}\lambda^2_{\max}(\boldsymbol{k}_j)$ hold, we have

$$\dot{V}_1 \leq -\sum_{i=1}^{N} \boldsymbol{S}_i^{\mathrm{T}} \boldsymbol{K}_{1i} \boldsymbol{S}_i \leq 0 \tag{29}$$

which implies that V_1 is asymptotically stable and bounded. Thus we can conclude that $\boldsymbol{S}_i$ and $\widetilde{\boldsymbol{\nu}}(\boldsymbol{\Xi}_i)$ are both bounded. Then, after time t_1 the following inequality holds: $\delta_i^k + |\boldsymbol{Y}_i(\boldsymbol{\xi}_i, \dot{\boldsymbol{\xi}}_i)\widetilde{\boldsymbol{\nu}}(\boldsymbol{\Xi}_i)|_k \leq \varphi_i^k, k = 1, 2, \ldots, 6$, where $\boldsymbol{\varphi}_i \in \mathbb{R}^{6\times 1}$ is a positive constant vector. Next, we consider the following Lyapunov function

$$V_2 = \sum_{i=1}^{N} \frac{1}{2}\boldsymbol{S}_i^{\mathrm{T}} \boldsymbol{M}_i \boldsymbol{S}_i = V_1 - \sum_{i=1}^{N} \frac{1}{2}\widetilde{\boldsymbol{\nu}}^{\mathrm{T}}(\boldsymbol{\Xi}_i)\boldsymbol{\Lambda}_i^{-1}\widetilde{\boldsymbol{\nu}}(\boldsymbol{\Xi}_i) \tag{30}$$

Calculating the derivative of V_2 with respect to time yields

$$\begin{aligned}
\dot{V}_2 &\leq -\sum_{i=1}^{N} \boldsymbol{S}_i^{\mathrm{T}} \boldsymbol{K}_{1i} \boldsymbol{S}_i - \sum_{i=1}^{N}\sum_{k=1}^{6} \left([\boldsymbol{K}_{2i}]_k - \delta_i^k\right)|\boldsymbol{S}_i^k| - \sum_{i=1}^{N}\sum_{j=1}^{N} \boldsymbol{\Upsilon}_{ij}^{\mathrm{T}}\boldsymbol{\Upsilon}_{ij} - \sum_{i=1}^{N}\sum_{j=1}^{N} \pounds_{ij}\boldsymbol{S}_j^{\mathrm{T}}\boldsymbol{S}_j + \sum_{i=1}^{N} \boldsymbol{Y}_i(\boldsymbol{\xi}_i, \dot{\boldsymbol{\xi}}_i)\widetilde{\boldsymbol{\nu}}(\boldsymbol{\Xi}_i)\boldsymbol{S}_i \\
&\leq -\sum_{i=1}^{N} \boldsymbol{S}_i^{\mathrm{T}} \boldsymbol{K}_{1i} \boldsymbol{S}_i - \sum_{i=1}^{N}\sum_{k=1}^{6} \left([\boldsymbol{K}_{2i}]_k - \varphi_i^k\right)|\boldsymbol{S}_i^k| \leq -\bar{a}_1 V_2 - \bar{a}_2 V_2^{1/2}
\end{aligned} \tag{31}$$

where $\bar{a}_1 = \min\left(2\lambda_{\min}(\boldsymbol{K}_{1i})/\lambda_{\max}(\boldsymbol{M}_i)\right) > 0$, and $\bar{a}_2 = \min\left(\sqrt{2}\,\|[\boldsymbol{K}_{2i}]_k - \varphi_i^k\|/\lambda_{\max}(\boldsymbol{M}_i)\right) > 0$. Thus by using Lemma 1, it is obvious that the sliding surface can be reached in finite time, which yields

$$\dot{\boldsymbol{\xi}}_i = -\boldsymbol{\vartheta}_{1i}\boldsymbol{\xi}_i - \boldsymbol{\vartheta}_{2i}\mathrm{sig}^{\alpha}(\boldsymbol{\xi}_i) \tag{32}$$

Next, in order to prove step 2, we consider another Lyapunov function $V_3 = \frac{1}{2}\boldsymbol{\xi}_i^{\mathrm{T}}\boldsymbol{\xi}_i$. Differentiating V_3 with respect to time and substituting Eq. (32) into it, we can obtain

$$\dot{V}_3 = \boldsymbol{\xi}_i^{\mathrm{T}}\dot{\boldsymbol{\xi}}_i = -\boldsymbol{\xi}_i^{\mathrm{T}}\left(\boldsymbol{\vartheta}_{1i}\boldsymbol{\xi}_i + \boldsymbol{\vartheta}_{2i}\mathrm{sig}^{\alpha}(\boldsymbol{\xi}_i)\right) \leq -\bar{\vartheta}_{1i}V_3 - \bar{\vartheta}_{2i}V_3^{\frac{1+\alpha}{2}} \tag{33}$$

where $\bar{\vartheta}_{1i} = 2\lambda_{\min}(\boldsymbol{\vartheta}_{1i}) > 0$ and $\bar{\vartheta}_{2i} = 2^{(1+\alpha)/2}\lambda_{\min}(\boldsymbol{\vartheta}_{2i}) > 0$. Thus by using Lemma 1, the finite-time stability of $\boldsymbol{\xi}_i$ is guaranteed. Then it is easy to obtain that $\dot{\boldsymbol{\xi}}_i = \boldsymbol{0}$ can also be reached in finite time. Thereby, the proof of Theorem 1 has been completed. □

Remark 2. In view of the proposed controller (24), it can be divided into three parts. The adaptive term $-\mathscr{B}_i^{-1}\boldsymbol{Y}_i(\boldsymbol{\xi}_i, \dot{\boldsymbol{\xi}}_i)\hat{\boldsymbol{\nu}}(\boldsymbol{\Xi}_i)$, which is used to control nominal components and drive the tracking errors of the followers to their reference states. The disturbance-rejection term $-\mathscr{B}_i^{-1}\left(\boldsymbol{K}_{1i}\boldsymbol{S}_i + \boldsymbol{K}_{2i}\mathrm{sgn}(\boldsymbol{S}_i)\right)$ is used to compensate for both lumped disturbances and estimation errors of inertia and mass to enhance the robustness of the SFF system. The formation control term $-\mathscr{B}_i^{-1}\sum_{j=1}^{N}(\boldsymbol{k}_{ij}\boldsymbol{S}_i - o_{ij}\boldsymbol{k}_j\boldsymbol{S}_j)$, which is used to maintain certain relative attitudes and formation configuration such that the SFF will perform as a whole within the formation. The controller is effective under any type of communication topology. Because a time varying binary number $o_{ij} = 0$ or 1 is used to describe the topology, the interconnection between each two followers can be disconnected or connected, fixed or time-varying. Moreover, since in the theoretical analysis of Theorem 1, we have no limits on $o_{ij} = o_{ji}$, thus if $o_{ij} = o_{ji}$ is satisfied for $\forall i, j \in N, i \neq j$, the topology is undirected, otherwise the topology will be directed.

Remark 3. For the sliding surface in (20), when $0 < \alpha < 1$, it will have the same form as the sliding surface in [21]. Though the surface has a high convergence either near the origin or far away from it, since its derivative includes $\mathrm{diag}(\mathrm{sig}^{\alpha-1}\boldsymbol{\xi}_i)\dot{\boldsymbol{\xi}}_i$ in $\boldsymbol{Y}_i(\boldsymbol{\xi}_i, \dot{\boldsymbol{\xi}}_i)$, the controller outputs will be infinite if $\boldsymbol{\xi}_i$ reaches the

origin before $\dot{\boldsymbol{\xi}}_i$. In this study, to improve the system transient state performance, we select $0.5 < \alpha < 1$ and keep $\boldsymbol{\xi}_i$ away from the origin before $\boldsymbol{S}_i = \boldsymbol{0}$ is reached such that no singularity will occur. Because when $\boldsymbol{S}_i = \boldsymbol{0}$, we have $\mathrm{diag}(\mathrm{sig}^{\alpha-1}\boldsymbol{\xi}_i)\dot{\boldsymbol{\xi}}_i = -\boldsymbol{\vartheta}_{1i}|\boldsymbol{\xi}_i|^{\alpha} - \boldsymbol{\vartheta}_{2i}\mathrm{sig}^{2\alpha-1}(\boldsymbol{\xi}_i) = 0$. Moreover, it should be noted that due to the implementation of the discontinuous sign function in controller (24), chattering appearing in control signals cannot be avoided, which is a common phenomenon in sliding mode controller design and is not desirable for engineering application. When applying sliding mode controller in practice, a continuous function $\boldsymbol{S}/(\|\boldsymbol{S}\| + \epsilon)$ is employed to approximate $\mathrm{sgn}(\boldsymbol{S})$ [17], where ϵ is a small positive constant.

3.2. Control law design with collision avoidance

It should be noted that collisions may occur among the followers in certain regions during the maneuver of driving the followers to their expected configurations, and the above proposed controller (24) fails to take the possible collisions into consideration. In order to solve the SFF control problem with collision avoidance, the artificial potential function method is adopted in this study. In $\mathscr{F}_I$, the relative position of ith follower to jth follower is $\boldsymbol{R}_{ij} = \boldsymbol{R}_i - \boldsymbol{R}_j$, and the distance between them is denoted as $r_{ij} = \|\boldsymbol{R}_{ij}\|$. Before proceeding, we introduce some concepts first. For the ith follower, we define a collision region $\boldsymbol{\Phi}_i = \{\boldsymbol{x} \in \mathbb{R}^{3\times 1} |\ \|\boldsymbol{x} - \boldsymbol{R}_i\| \leq r_c\}$, where r_c is the minimum safe distance between the followers to meet the requirement of collision avoidance. Moreover, an avoidance region $\boldsymbol{\Psi}_i = \{\boldsymbol{x} \in \mathbb{R}^{3\times 1} |\ r_c < \|\boldsymbol{x} - \boldsymbol{R}_i\| \leq r_a\}$ is defined, in which the designed collision avoidance schemes are activated to avoid collisions. In the avoidance region, the ability of each follower measuring its relative distances with respect to the others should be promised. Thus the communication topology should be redefined as:

$$o_{ij}(\mathrm{CA}) = \begin{cases} 1, & r_c < r_{ij} \leq r_a, \\ o_{ij}, & r_{ij} > r_a. \end{cases} \tag{34}$$

Generally speaking, the concept of potential field comes from the physical model of molecular interaction: the Lennard-Jones potential [5]. The field has its global minimum at the desired position of the object and will have high values once the object is in the forbidden areas [32]. Therefore, we use the gradient of the potential field to measure the magnitude of the repulsive force to prevent the followers from colliding with each other. The designed potential function $U(r_{ij})$ should be nonnegative and its derivative should be nonpositive, and both of them should be continuous at $r_{ij} = r_a$, which satisfies:

1. $U(r_{ij}) = 0, r_{ij} \in (r_a, +\infty)$; 2. $U^{'}(r_{ij}) = 0, r_{ij} \in (r_a, +\infty)$; 3. $\lim\limits_{r_{ij}\to r_a^-} U(r_{ij}) = \lim\limits_{r_{ij}\to r_a^+} U(r_{ij}) = 0$;
4. $\lim\limits_{r_{ij}\to r_a^-} U^{'}(r_{ij}) = \lim\limits_{r_{ij}\to r_a^+} U^{'}(r_{ij}) = 0$; 5. $U(r_{ij}) > 0, r_{ij} \in (r_c, r_a)$; 6. $U^{'}(r_{ij}) < 0, r_{ij} \in (r_c, r_a)$;
7. $\lim\limits_{r_{ij}\to r_c^+} U(r_{ij}) = +\infty$; 8. $\lim\limits_{r_{ij}\to r_c^+} U^{'}(r_{ij}) = -\infty$.

The potential function designed in this study is motivated by [28, 30] and given as follows:

$$U(r_{ij}) = \begin{cases} \Big(\dfrac{r_a^2 - \|\boldsymbol{R}_i - \boldsymbol{R}_j\|^2}{\|\boldsymbol{R}_i - \boldsymbol{R}_j\|^2 - r_c^2}\Big)^2, & r_c < r_{ij} \leq r_a \\ 0, & r_{ij} > r_a \end{cases} \tag{35}$$

Taking its partial derivative with respect to $\boldsymbol{R}_i$, yields

$$\frac{\partial U(r_{ij})}{\partial \boldsymbol{R}_i} = \begin{cases} -\Big(\dfrac{4(r_a^2 - r_c^2)(r_a^2 - \|\boldsymbol{R}_i - \boldsymbol{R}_j\|^2)}{(\|\boldsymbol{R}_i - \boldsymbol{R}_j\|^2 - r_c^2)^3}\Big)(\boldsymbol{R}_i - \boldsymbol{R}_j)^{\mathrm{T}}, & r_c < r_{ij} \leq r_a. \\ 0, & r_{ij} > r_a. \end{cases} \tag{36}$$

Then the controller (24) in consideration of collision avoidance can be modified as

$$\boldsymbol{\Gamma}_{\mathrm{ci}}^{*}=\boldsymbol{\Gamma}_{\mathrm{ci}}-\mathscr{B}_{i}^{-1}[\mathbf{0}_{1\times3},K_{cai}\sum_{j=1}^{n}\frac{\partial U(r_{ij})}{\partial\boldsymbol{R}_{i}}\boldsymbol{C}_{i}]^{\mathrm{T}} \tag{37}$$

where K_{cai} is a positive scalar and n is the number of followers in the avoidance region $\boldsymbol{\Psi}_i$.

Denoting $\boldsymbol{a}_{cai}=[\mathbf{0}_{1\times3},-K_{cai}\sum_{j=1}^{n}\frac{\partial U(r_{ij})}{\partial\boldsymbol{R}_{i}}\boldsymbol{C}_{l}]^{\mathrm{T}}$ and taking this modified controller into Eq. (23), yields

$$\boldsymbol{M}_{i}\dot{\boldsymbol{S}}_{i}+\boldsymbol{H}_{i}\boldsymbol{S}_{i}=\boldsymbol{Y}_{i}(\boldsymbol{\xi}_{i},\dot{\boldsymbol{\xi}}_{i})\boldsymbol{\nu}(\boldsymbol{\Xi}_{i})+\mathscr{B}_{i}\boldsymbol{\Gamma}_{\mathrm{ci}}+\Delta\boldsymbol{d}_{i}+\boldsymbol{a}_{cai} \tag{38}$$

Theorem 2. *For the SFF system governed by Eq. (38), Assumptions 1 is satisfied and all the SFF members are outside each other's collision region $\boldsymbol{\Phi}_i$ at $t=0$. The controller is designed as Eq. (37), the adaptive law is given by Eq. (25), and all the control parameters in $\boldsymbol{\Gamma}_{\mathrm{ci}}$ are the same as those defined in Theorem 1 with $\lambda_{\min}(\boldsymbol{k}_{ij})>\hbar_{ij}$, $[\boldsymbol{K}_{2i}]_k>\varphi_i^k$, and $\hbar_{ij}(4\lambda_{\min}(\boldsymbol{k}_{ij})-\hbar_{ij})\geqslant o_{ij}(\mathrm{CA})\lambda_{\max}^{2}(\boldsymbol{k}_j)$ holding. If the collision avoidance parameters are designed such that*

$$\|\boldsymbol{a}_{cai}\|<\frac{\lambda_{\min}(\boldsymbol{K}_1)\|\bar{\boldsymbol{S}}\|\lambda_{\min}(\boldsymbol{M})}{N\lambda_{\max}(\boldsymbol{M})} \tag{39}$$

then the finite-time stability of the closed-loop SFF system can be guaranteed. Furthermore, during the formation maneuver collision avoidance can be guaranteed.

Proof. In order to prove the stability of the resulting closed-loop SFF system, we first rewrite Eq. (38) as follows:

$$\boldsymbol{M}\dot{\bar{\boldsymbol{S}}}+\boldsymbol{H}\bar{\boldsymbol{S}}=\boldsymbol{Y}\boldsymbol{\nu}+\boldsymbol{B}\boldsymbol{\Gamma}_{\mathrm{c}}+\Delta\boldsymbol{d}+\boldsymbol{a}_{ca} \tag{40}$$

where

$\bar{\boldsymbol{S}}=[\boldsymbol{S}_1^{\mathrm{T}},\boldsymbol{S}_2^{\mathrm{T}},\cdots,\boldsymbol{S}_N^{\mathrm{T}}]^{\mathrm{T}}\in\mathbb{R}^{6N\times1}$, $\boldsymbol{M}=\mathrm{diag}(\boldsymbol{M}_1,\boldsymbol{M}_2,\ldots,\boldsymbol{M}_N)\in\mathbb{R}^{6N\times6N}$,
$\boldsymbol{Y}\boldsymbol{\nu}=[(\boldsymbol{Y}_1\boldsymbol{\nu}_1)^{\mathrm{T}},\ldots,(\boldsymbol{Y}_N\boldsymbol{\nu}_N)^{\mathrm{T}}]^{\mathrm{T}}\in\mathbb{R}^{6N\times1}$, $\boldsymbol{H}=\mathrm{diag}(\boldsymbol{H}_1,\boldsymbol{H}_2,\ldots,\boldsymbol{H}_N)\in\mathbb{R}^{6N\times6N}$,
$\boldsymbol{B}=\mathrm{diag}(\mathscr{B}_1,\mathscr{B}_2,\ldots,\mathscr{B}_N)\in\mathbb{R}^{6N\times6N}$, $\boldsymbol{\Gamma}_{\mathrm{c}}=[\boldsymbol{\Gamma}_{\mathrm{c1}}^{\mathrm{T}},\boldsymbol{\Gamma}_{\mathrm{c2}}^{\mathrm{T}},\ldots,\boldsymbol{\Gamma}_{\mathrm{cN}}^{\mathrm{T}}]^{\mathrm{T}}\in\mathbb{R}^{6N\times1}$,
$\boldsymbol{a}_{ca}=[\boldsymbol{a}_{ca1}^{\mathrm{T}},\boldsymbol{a}_{ca2}^{\mathrm{T}},\ldots,\boldsymbol{a}_{caN}^{\mathrm{T}}]^{\mathrm{T}}\in\mathbb{R}^{6N\times1}$.

Then we can write the system in the form of the perturbed system as defined in Definition 1

$$\dot{\bar{\boldsymbol{S}}}=\boldsymbol{f}(t,\bar{\boldsymbol{S}})+\boldsymbol{g}(t,\bar{\boldsymbol{S}}) \tag{41}$$

where $\boldsymbol{f}(t,\bar{\boldsymbol{S}})=\boldsymbol{M}^{-1}(-\boldsymbol{H}\bar{\boldsymbol{S}}+\boldsymbol{Y}\boldsymbol{\nu}+\boldsymbol{B}\boldsymbol{\Gamma}_{\mathrm{c}}+\Delta\boldsymbol{d})$, $\boldsymbol{g}(t,\bar{\boldsymbol{S}})=\boldsymbol{M}^{-1}\boldsymbol{a}_{ca}$.

Next, based on the above definitions, for the nominal system $\dot{\bar{\boldsymbol{S}}}=\boldsymbol{f}(t,\bar{\boldsymbol{S}})$, taking the derivative of $V_2=\frac{1}{2}\bar{\boldsymbol{S}}^{\mathrm{T}}\boldsymbol{M}\bar{\boldsymbol{S}}$ with respect to time as the same proof process in Theorem 1, we can obtain

$$\dot{V}_2\leq-\lambda_{\min}(\boldsymbol{K}_1)\|\bar{\boldsymbol{S}}\|^2-\bar{\mu}\|\bar{\boldsymbol{S}}\| \tag{42}$$

where $\boldsymbol{K}_1=\mathrm{diag}(\boldsymbol{K}_{11},\ldots,\boldsymbol{K}_{1N})$, $\bar{\mu}=\min([\boldsymbol{K}_{2i}]_k-\varphi_i^k),i=1,2,\ldots,N.\ k=1,2,\ldots,6$. And for the vanishing perturbation $\boldsymbol{g}(t,\bar{\boldsymbol{S}})$, we have

$$\|\boldsymbol{g}(t,\bar{\boldsymbol{S}})\|=\|\boldsymbol{M}^{-1}\boldsymbol{a}_{ca}\|\leq\|\boldsymbol{M}^{-1}\|\sum_{i=1}^{N}\|\boldsymbol{a}_{cai}\|\leq\frac{\sum_{i=1}^{N}\|\boldsymbol{a}_{cai}\|}{\lambda_{\min}(\boldsymbol{M})} \tag{43}$$

If the condition in Eq. (39) is satisfied, $\|\boldsymbol{g}(t,\bar{\boldsymbol{S}})\|<\frac{\lambda_{\min}(\boldsymbol{K}_1)}{\lambda_{\max}(\boldsymbol{M})}\|\bar{\boldsymbol{S}}\|$ holds. By choosing $0<\beta_1\leq0.5\lambda_{\min}(\boldsymbol{M})$, $\beta_2\geqslant0.5\lambda_{\max}(\boldsymbol{M})$, $\beta_3=\lambda_{\min}(\boldsymbol{K}_1)$, $\beta_4=\bar{\mu}$, $\beta_5=\lambda_{\max}(\boldsymbol{M})$, $\gamma=0.5$, and $\kappa<\frac{\lambda_{\min}(\boldsymbol{K}_1)}{\lambda_{\max}(\boldsymbol{M})}=\beta_3/\beta_5$, the conditions in Lemma 2 will all be satisfied. Then $\bar{\boldsymbol{S}}$ will converge to the origin in finite-time. In combination

with the proof process of step 2 in Theorem 1, the finite-time stability of $\dot{\boldsymbol{\xi}}_i, \boldsymbol{\xi}_i$ can be guaranteed. The overall analysis completes the proof of Theorem 2. □

Remark 4. For the modified controller, the term $\boldsymbol{a}_{cai}$ is used to avoid collisions. Since the direction of $-\frac{\partial U(r_{ij})}{\partial \boldsymbol{R}_i}$ is from jth follower to ith follower, when follower j is in $\boldsymbol{\Psi}_i$, a repulsive force will be generated on follower i such that follower j will move away from the forbidden area relatively. Moreover, it should be noted that the collision avoidance schemes are effective only when Eq. (39) is satisfied. Usually, for certain shapes of the SFF followers, the value of r_c is fixed , and r_a and K_{cai} can be adjusted according to the requirements of specific aerospace missions to satisfy Eq. (39). The lager of K_{cai} and the closer of r_a to r_c are, the larger collision avoidance acceleration will be generated. However, since in the proof of Theorem 2, the collision avoidance acceleration is regarded as the vanishing perturbation of the SFF system, if its value is too large, maybe the control performance would be sacrificed. Thus some compromises should be considered in the process of parameters design.

4. Simulation results

In this section, numerical examples are conducted to verify the effectiveness of the proposed finite-time controller for a given SFF mission scenario, in which a virtual leader and four followers are involved. The nominal parts of the mass of the followers are assumed to be: $m_1 = 100\text{kg}$, $m_2 = 105\text{kg}$, $m_3 = 108\text{kg}$ and $m_4 = 110\text{kg}$, and the nominal parts of the inertia matrices ($\text{kg} \cdot \text{m}^2$) are

$$\boldsymbol{J}_1 = \begin{bmatrix} 25 & 1 & 0.5 \\ 1 & 22 & 1.2 \\ 0.5 & 1.2 & 23 \end{bmatrix}; \boldsymbol{J}_2 = \begin{bmatrix} 22 & 1.5 & 1 \\ 1.5 & 26 & -1.2 \\ 1 & -1.2 & 28 \end{bmatrix};$$
$$\boldsymbol{J}_3 = \begin{bmatrix} 28 & 1.2 & 1.6 \\ 1.2 & 27 & -1.5 \\ 1.6 & -1.5 & 25 \end{bmatrix}; \boldsymbol{J}_4 = \begin{bmatrix} 30 & 1.5 & 2 \\ 1.5 & 25 & 1.3 \\ 2 & 1.3 & 26 \end{bmatrix}.$$

It should be noted that the virtual leader is only used to generate the desired trajectory, thus its mass and inertia can be arbitrary values. For convenience, we assume that $m_l = 100\text{kg}$ and $\boldsymbol{J}_l = \text{diag}(20, 20, 20)\text{kg}\cdot\text{m}^2$. The mission is that four followers are involved in the SFF system, and it is desired to reconfigure them to a circle-shaped formation with their coordinates being $\boldsymbol{\rho}_1^d = [0, -25, 0]^{\mathrm{T}}\text{m}$, $\boldsymbol{\rho}_2^d = [25, 0, 0]^{\mathrm{T}}\text{m}$, $\boldsymbol{\rho}_3^d = [0, 25, 0]^{\mathrm{T}}\text{m}$, $\boldsymbol{\rho}_4^d = [-25, 0, 0]^{\mathrm{T}}\text{m}$ expressed in $\mathscr{F}_o$ with respect to the virtual leader, whose orbital elements are given in Table 1. While, the attitude, the angular velocity and the translational velocity of the virtual leader need to be tracked by each follower.

Table 1: Initial orbital elements of the virtual leader.

Orbital parameters	Values
Semi-major axis	6778.14km
Eccentricity	0
Inclination	45°
Argument of perigee	-150°
Mean anomaly	270°
Right ascension of ascending node (RAAN)	-60°

Table 2: Initial tracking errors of the followers.

Initial States	Parameter Values
Initial relative positions (m)	$\boldsymbol{\rho}_1(t_0) = [15\sqrt{2}, 12, -15\sqrt{3}]^{\mathrm{T}}$, $\boldsymbol{\rho}_2(t_0) = [-10\sqrt{3}, -15\sqrt{2}, 15]^{\mathrm{T}}$, $\boldsymbol{\rho}_3(t_0) = [15, -10\sqrt{3}, -15\sqrt{2}]^{\mathrm{T}}$, $\boldsymbol{\rho}_4(t_0) = [10, -5\sqrt{2}, 10]^{\mathrm{T}}$.
Initial relative attitudes	$\boldsymbol{\sigma}_{e1} = [0.44, 0.26, -0.51]^{\mathrm{T}}$, $\boldsymbol{\sigma}_{e2} = [0.51, 0.14, -0.29]^{\mathrm{T}}$, $\boldsymbol{\sigma}_{e3} = [0.41, 0.2, -0.57]^{\mathrm{T}}$, $\boldsymbol{\sigma}_{e4} = [0.37, 0.3, -0.7]^{\mathrm{T}}$.
Initial relative velocities	$\dot{\boldsymbol{\rho}}_i = \dot{\boldsymbol{\sigma}}_{ei} = \mathbf{0}$

Initially, the followers are assumed to be performing a different mission, and there are already some proper controls acting on them to obtain the initial relative states with respect to the virtual leader as presented in Table 2. During the process of driving the followers to their desired states, the disturbance forces and torques considering solar radial pressure force, magnetic torque, and aerodynamics that the followers suffer are assumed to be [32, 36]:

$$\boldsymbol{d}_{\tau i} = 10^{-4} \cdot \begin{bmatrix} \sin(i + 0.12t) \\ \cos(i + 0.15t) \\ \sin(i + 0.18t) \end{bmatrix} (\mathrm{N} \cdot \mathrm{m}),$$

$\boldsymbol{d}_{fi} = 10^{-5} \cdot [\ -1.025,\ 6.248,\ -2.215\ ]^{\mathrm{T}} \sin(2\pi \|\boldsymbol{\omega}_l\| t)$ (N).

The uncertainty parts of mass and inertia matrix considering fuel cost are chosen as $\Delta\boldsymbol{\Xi}_i = \mathrm{diag}(0.2\boldsymbol{J}_i, 0.2m_i\boldsymbol{I}_3)$, and the changing communication topologies o_{ij} are set as

$$\begin{aligned} o_{12} &= o_{13}(t+1.2) = o_{14}(t-3.5) = o_{21}(t+4.8) = o_{23}(t-2.6) = o_{24}(t-1.6) = o_{31}(t-4.5) \\ &= o_{32}(t+5.2) = o_{34}(t-1) = o_{41}(t-5.5) = o_{42}(t+2.2) = o_{43}(t-2.4) \end{aligned}$$

where $o_{12}(t) = \begin{cases} 1 & \mathrm{mod}\ (t, 8) \le 6 \\ 0 & \mathrm{mod}\ (t, 8) > 6 \end{cases}$, and mod(t, 8) represents the remainder of dividing t by 8.

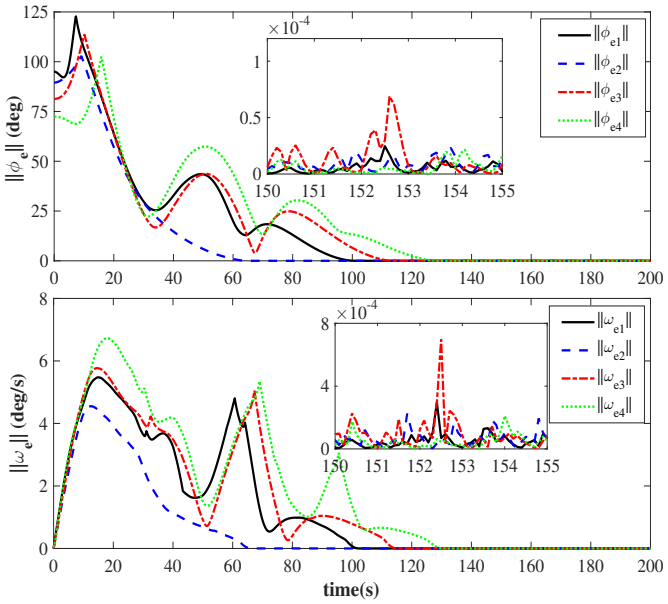

Fig. 2. Case 1: Norms of attitude and angular velocity tracking errors.

Three cases are considered: Case 1: the proposed controller (37) with collision avoidance schemes and coordination terms; Case 2: without collision avoidance schemes; and Case 3: without coordina-

tion terms. Each follower is modeled as a sphere with radius 6m, and then it is suitable to choose $r_c = 12$m, and modify the communication topology as o_{ij}(CA) in Eq. (34). The guideline of choosing the controller parameters for these cases is by trial-and-error until a good control performance is obtained, and the controller parameters are chosen as: $\boldsymbol{K}_{1i} = \text{diag}(5\boldsymbol{I}_3, 6\boldsymbol{I}_3)$, $\boldsymbol{K}_{2i} = \text{diag}(0.15\boldsymbol{I}_3, 0.2\boldsymbol{I}_3)$, $\boldsymbol{\vartheta}_{1i} = \text{diag}(0.06\boldsymbol{I}_3, 0.03\boldsymbol{I}_3)$, $\boldsymbol{\vartheta}_{2i} = \text{diag}(0.08\boldsymbol{I}_3, 0.05\boldsymbol{I}_3)$, $\alpha = 2/3$, $r_a = 25$m, $K_{cai} = 1.2$, $\boldsymbol{k}_{ij} = 2\boldsymbol{I}_6$, $\boldsymbol{k}_j = 0.8\boldsymbol{I}_6$, $\boldsymbol{\Lambda}_i = \text{diag}(12, 12, 12, 12, 12, 12, 1.5)$, and the initial estimations of $\hat{\boldsymbol{\nu}}(\boldsymbol{\Xi}_i)$ are all set as $[25, 25, 25, 0, 0, 0, 100]^{\mathrm{T}}$. In addition, special attention should be paid to actuator saturation due to physical limits. Here, we assume that the followers have available continuous control outputs in all body axes. The control torques are generated by reaction wheels with maximum torque $\boldsymbol{\tau}_{\max} = 0.2\text{N}\cdot\text{m}$ [36], and the control forces are provided by thrusters with maximum output $\boldsymbol{u}_{\max} = 5$N [32], respectively. If the theoretical control input is larger than the maximum value, then the actual control input will be described as [7]: $\text{sat}(\boldsymbol{\tau}_i^{k=1,2,3}) = \text{sign}(\boldsymbol{\tau}_i^k)\min\{|\boldsymbol{\tau}_i^k|, \boldsymbol{\tau}_{\max}\}$ and $\text{sat}(\boldsymbol{u}_i^{k=4,5,6}) = \text{sign}(\boldsymbol{u}_i^k)\min\{|\boldsymbol{u}_i^k|, \boldsymbol{u}_{\max}\}$. Case 2 with $K_{cai} = 0$ and Case 3 with $\boldsymbol{k}_{ij} = \boldsymbol{k}_j = \boldsymbol{0}$ are conducted for the purpose of comparison to highlight the proposed controller. Simulation results are presented in Figs. 2-10.

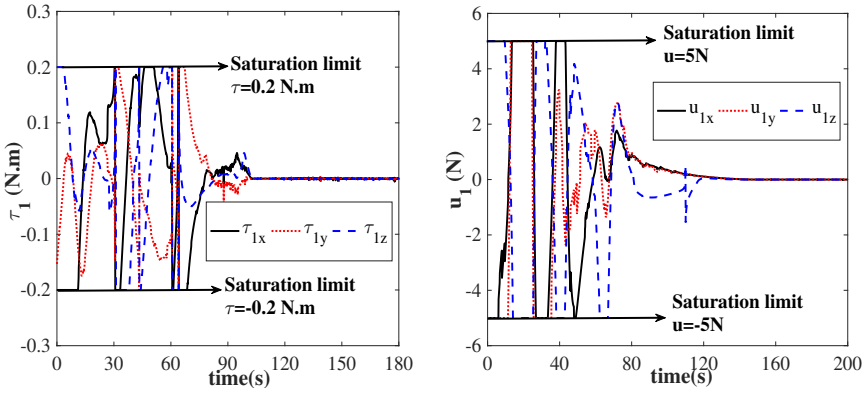

Fig. 3. Case 1: Time responses of control torques (left) and control forces (right).

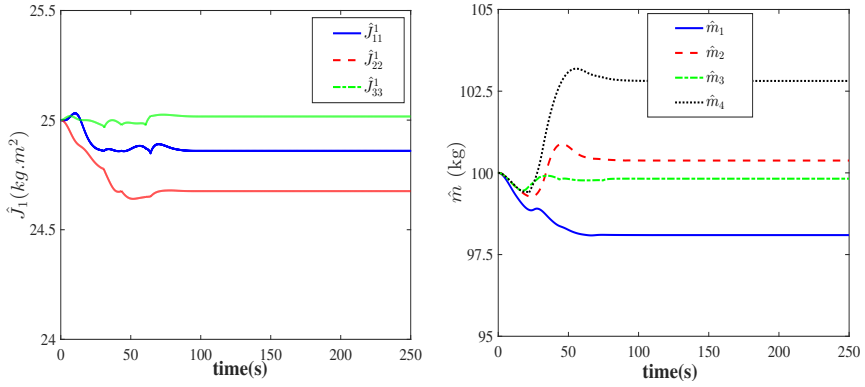

Fig. 4. Case 1: Parameter estimations for $\hat{\boldsymbol{\nu}}(\boldsymbol{\Xi}_i)$.

Fig. 2 shows the time histories of attitude synchronization, including norms of error Euler principal angles, which can be obtained as in [35], and norms of relative angular velocities of Case 1. It can be seen that the rotational motion of the leader is synchronized by the followers with a settling time less than 130s. The steady-state errors show that the proposed controller has fine performance with $\|\phi_{ei}\| < 1 \times 10^{-4}$(deg) and $\|\omega_{ei}\| < 8 \times 10^{-4}$(deg/s). The corresponding applied control torques and forces on the followers are

presented in Fig. 3, from which we can see that the control outputs are bounded by actuator saturation. Fig. 4 shows the response of the estimated values of the adaptive parameters in controller (24). For the sake of brevity, only the plots of the control torques and forces of follower 1, and $\hat{\boldsymbol{J}}_1$ are provided. Although the estimated values do not converge to their true values, using these values as the feedback states of the controller, the finite-time stability of the SFF system is still promised.

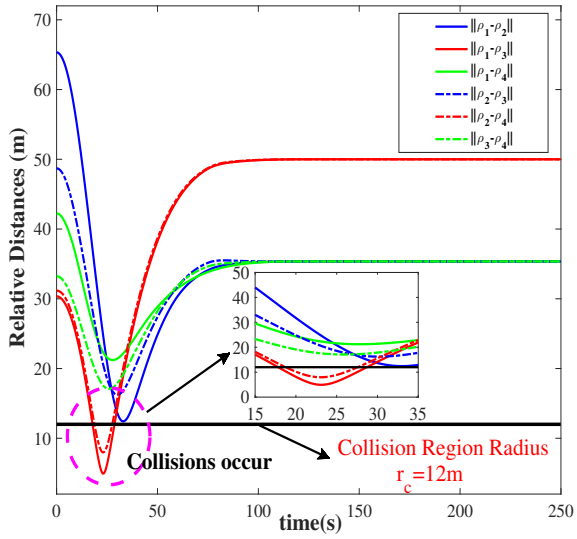

Fig. 5. Relative distances of the followers without collision avoidance schemes in formation.

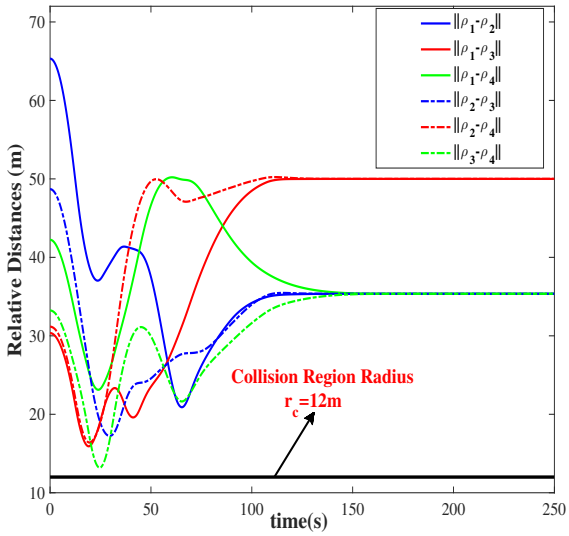

Fig. 6. Relative distances of the followers with collision avoidance schemes in formation.

The results presented in Figs. 5-7 are used to demonstrate the effectiveness of the collision avoidance schemes. Fig. 5 presents the time histories of the relative distances between each two followers of the SFF without collision avoidance schemes, and the plots with collision avoidance schemes are given in Fig. 6. We can see that without the collision avoidance schemes, follower 1 and 3, follower 2 and 4 will collide with each other during the formation reconfiguration maneuver. When applying the proposed collision avoidance

schemes, the safety of the formation can be guaranteed as illustrated in Fig. 6. Meanwhile, in both cases, the followers will arrive their desired relative positions, but the settling time of Case 1 is about 135s and that of Case 2 is less than 100s. The norms of the position tracking errors and the norms of translational velocity tracking errors of each follower with respect to their desired states without and with collision avoidance schemes are given in Fig. 7. It can be seen that the convergence time, the transient process and the steady-state errors of Case 2 are better than those of Case 1. Moreover, to compare the performance of these two cases further, the corresponding applied control force of follower 1 in case 2 is presented in Fig. 8. Furthermore, the fuel is always limited for on-orbit spacecraft , which means that energy-efficient issue as a key to extend spacecraft's working life should be considered seriously in the comparison. Thus, we define the energy cost function as $\boldsymbol{E} = \int_0^{\mathrm{T}} \|\boldsymbol{u}_i\|^2 \, dt$ to compare the performance of Case 1 and Case 2 more deeply, where T is set to be 200s. Time responses of the energy consumption of these two cases are presented in Fig. 9, and CA is the abbreviation of collision avoidance. From the results of Figs. 3, 7-9 we can conclude that the safety of the SFF system is guaranteed at the cost of control performance and more energy, and considering some compromises in the process of controller parameters design is necessary, as illustrated in Remark 4.

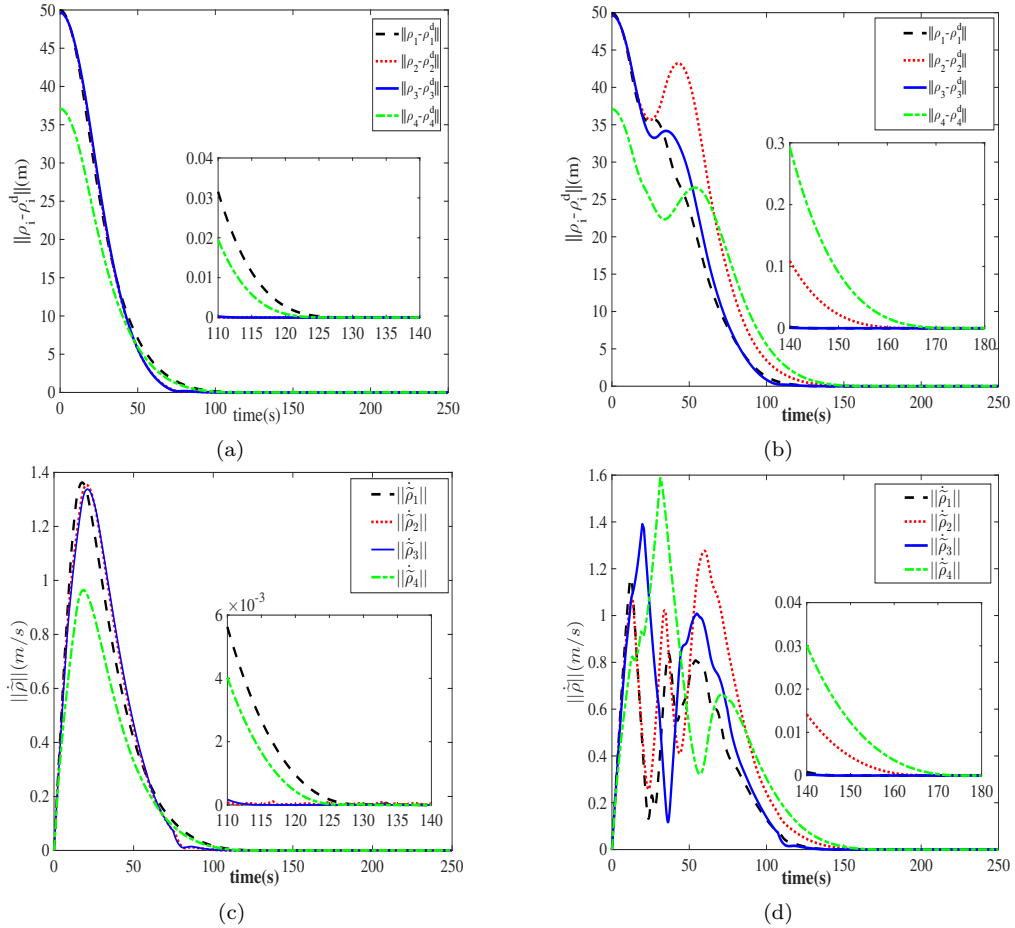

Fig. 7. Norms of (a) position tracking errors without collision avoidance schemes, (b) position tracking errors with collision avoidance schemes, (c) translational velocity tracking errors without collision avoidance schemes, (d) translational velocity tracking errors with collision avoidance schemes.

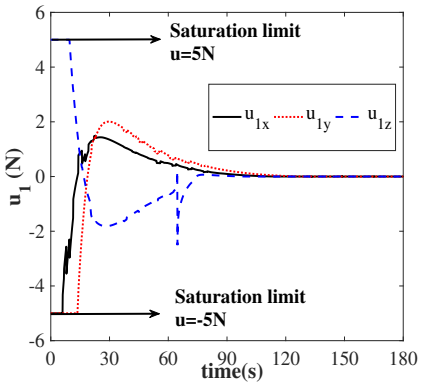

Fig. 8. Case 2: Time responses of control forces

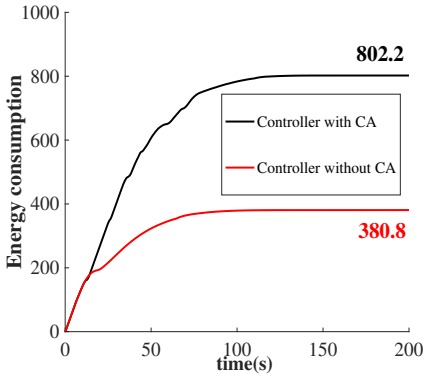

Fig. 9. Energy consumption comparison between Case 1 and 2

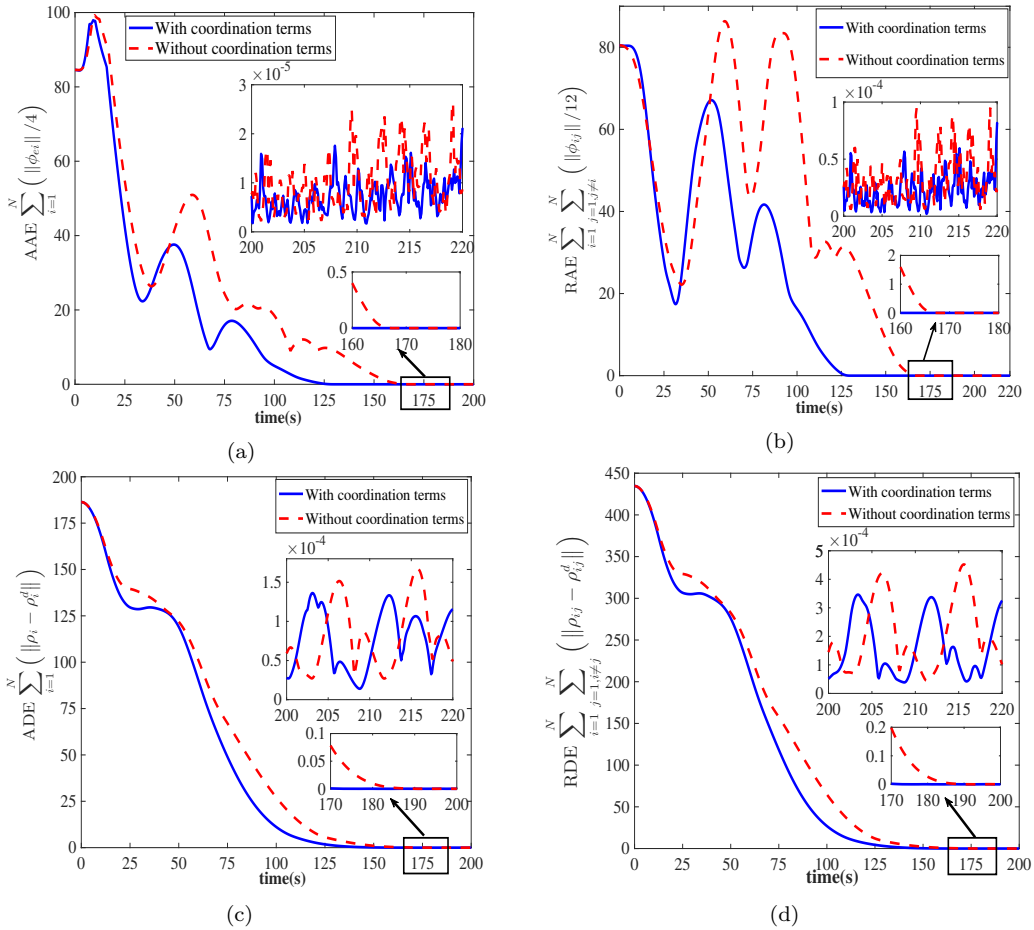

Fig. 10. Time responses of rotational and translational motion performance indexes (a) AAE, (b) RAE, (c) ADE, (d) RDE.

Finally, to show the proposed controller (37) can promise a better control performance of formation-keeping and relative attitude consensus among followers when the position tracking maneuver and absolute attitude synchronization are performed, comparisons between the simulation results of Case 1 and Case 3 are presented. Four performance indexes: absolute attitude errors (AAE), relative attitude errors (RAE), absolute distance errors (ADE), and relative distance errors (RDE) are introduced herein to measure the

performance, defined as:

$$\text{AAE} = \sum_{i=1}^{N} \big(\|\boldsymbol{\phi}_{ei}\|/4\big);\ \text{RAE} = \sum_{i=1}^{N}\sum_{j=1,j\neq i}^{N} \big(\|\boldsymbol{\phi}_{ij}\|/12\big);$$
$$\text{ADE} = \sum_{i=1}^{N} \big(\|\boldsymbol{\rho}_i - \boldsymbol{\rho}_i^d\|\big); \text{RDE} = \sum_{i=1}^{N}\sum_{j=1,j\neq i}^{N} \big(\|\boldsymbol{\rho}_{ij} - \boldsymbol{\rho}_{ij}^d\|\big).$$

The curves of AAE, RAE, ADE, and RDE are given in Fig. 10. It can be observed that the convergent accuracy of these four indexes is AAE $< 3 \times 10^{-5}$(deg), RAE $< 1 \times 10^{-4}$(deg), ADE $< 1.5 \times 10^{-4}$m and RDE $< 5 \times 10^{-4}$m. Though the accuracy of Case 3 is only a little worse than Case 1, the convergence time and the transient process of controller (37) involving the coordination terms are much better than the controller of Case 3 without coordination terms. Summarizing the comparison results of the above three cases, we can conclude that the existence of the collision avoidance schemes enhances the safety of the SFF system, and by introducing the coordination terms in controller (37), the control objective of this study can be achieved with fine performance.

5. Conclusions

In this paper, a relative motion control problem for six-degree-of-freedom spacecraft formation flying was solved. The developed decentralized control law was robust to model uncertainties and external disturbances, and guaranteed convergence to the desired formation in finite-time. In addition, the collision avoidance schemes were effective to avoid collisions during the formation reconfiguration maneuver. Furthermore, the controller only required the bounds of the inertia and mass of each follower and was effective for all types of topology: disconnected or connected, fixed or time-varying, and directed or undirected. Finally, numerical examples for a given mission scenario were conducted to show the effectiveness of the proposed controller. The simulation results of three cases have shown that the investigated problem in this study could be solved effectively by the presented controller, and the existence of coordination terms in the controller promised faster convergence time (about 135s) and a better performance of the transient process of formation tracking and attitude consensus maneuver than the controller without coordination terms (about 180s). While, since collision avoidance was achieved at the cost of control performance and more energy, some compromises considered in controller design for different missions would be necessary.

6. Acknowledgements

This work was supported by China Scholarship Council, the National Natural Science Foundation of China (Grant No. 61603115, 91438202, 91638301), China Postdoctoral Science Foundation (Grant No. 2015M81455) and the Heilongjiang Postdoctoral Fund (Grant No. LBH-Z15085).

7. References

[1] J. Wang, H. Liang, Z. Sun, et al, Finite-time control for spacecraft formation with dual-number-based description, Journal of Guidance Control and Dynamics 35 (3) (2012) 950–962.
[2] R. Sun, J. Wang, D. Zhang, X. Shao, Neural network-based sliding mode control for atmospheric-actuated spacecraft formation using switching strategy, Advances in Space Research 61 (2018) 914–926.
[3] H. Xu, Y. Ye, Z. Yang, Analytical solutions to optimal underactuated spacecraft formation reconfiguration, Advances in Space Research 56 (2015) 2151–2166.
[4] A. M. Zou, A. H. J. D. Ruiter, K. D. Kumar, Distributed finite-time velocity-free attitude coordination control for spacecraft formations, Automatica 67 (2016) 46–53.
[5] D. Lee, A. K. Sanyal, E. A. Butcher, Asymptotic tracking control for spacecraft formation flying with decentralized collision avoidance, Journal of Guidance, Control, and Dynamics 38 (4) (2014) 587–600.
[6] D. Ye, J. Zhang, Z. Sun, Extended state observer based finite-time controller design for coupled spacecraft formation with actuator saturation, Advances in Mechanical Engineering 9 (4) (2017) 1687814017696413.
[7] C. Liu, G. Vukovich, K. Shi, Z. Sun, Robust fault tolerant nonfragile h_∞ attitude control for spacecraft via stochastically intermediate observer, Advances in Space Research 62 (2018) 2631–2648.

[8] J. Xu, P. Shi, C. C. Lim, C. Cai, Y. Zou, Reliable tracking control for under-actuated quadrotors with wind disturbances, IEEE Transactions on Systems Man and Cybernetics Systems PP (99) (2018) 1–12.
[9] Q. Zhou, C. Wu, P. Shi, Observer-based adaptive fuzzy tracking control of nonlinear systems with time delay and input saturation, Fuzzy Sets and Systems 316 (2017) 49–68.
[10] H. Yang, P. Shi, X. Zhao, Y. Shi, Adaptive output-feedback neural tracking control for a class of nonstrict-feedback nonlinear systems, Information Sciences 334-335 (2016) 205–218.
[11] J. Sun, S. Song, G. Wu, Tracking control via robust dynamic surface control for hypersonic vehicles with input saturation and mismatched uncertainties, International Journal of Innovative Computing, Information and Control 13 (6) (2017) 2067–2087.
[12] D. Spiller, K. Basu, F. Curti, C. Circi, On the optimal passive formation reconfiguration by using attitude control, Acta Astronautica (https://doi.org/10.1016/j.actaastro.2018.01.052).
[13] J. Zhang, D. Ye, Z. Sun, C. Liu, Extended state observer based robust adaptive control on se(3) for coupled spacecraft tracking maneuver with actuator saturation and misalignment, Acta Astronautica 143 (2018) 221–233.
[14] L. Sun, Z. Zheng, Adaptive relative pose control for autonomous spacecraft rendezvous and proximity operations with thrust misalignment and model uncertainties, Advances in Space Research 59 (2017) 1861–1871.
[15] F. Zhang, G. Duan, Robust adaptive integrated translation and rotation control of a rigid spacecraft with control saturation and actuator misalignment, Acta Astronautica 86 (3) (2013) 167–187.
[16] H. Gui, G. Vukovich, Dual-quaternion-based adaptive motion tracking of spacecraft with reduced control effort, Nonlinear Dynamics 83 (1-2) (2015) 597–614.
[17] B. Xiao, S. Yin, L. Wu, A structure simple controller for satellite attitude tracking maneuver, IEEE Transactions on Industrial Electronics 64 (2) (2017) 1436–1446.
[18] B. Q. Zhang, S. M. Song, X. L. Chen, Decentralized robust coordinated control for formation flying spacecraft with coupled attitude and translational dynamics, Proceedings of Institution of Mechanical Engineers Part G Journal of Aerospace Engineering 227 (5) (2013) 798–815.
[19] B. Xiao, Q. Hu, Y. Zhang, Finite-time attitude tracking of spacecraft with fault-tolerant capability, IEEE Transactions on Control Systems Technology 23 (4) (2015) 1338–1350.
[20] H. Gui, G. Vukovich, Distributed almost global finite-time attitude consensus of multiple spacecraft without velocity measurements, Aerospace Science and Technology 75 (2018) 284–296.
[21] S. N. Wu, X. Y. Sun, Z. W. Sun, C. C. Chen, Robust sliding mode control for spacecraft global fast-tracking manoeuvre, Proceedings of the Institution of Mechanical Engineers Part G Journal of Aerospace Engineering 225 (G7) (2011) 749–760.
[22] R. Liu, X. Cao, M. Liu, Finite-time synchronization control of spacecraft formation with network-induced communication delay, IEEE Access 5 (2017) 27242–27253.
[23] D. Lee, G. Vukovich, H. Gui, Adaptive variable-structure finite-time mode control for spacecraft proximity operations with actuator saturation, Advances in Space Research 59 (10) (2017) 2473–2487.
[24] D. Lee, G. Vukovich, Adaptive finite-time control for spacecraft hovering over an asteroid, IEEE Transactions on Aerospace and Electronic Systems 52 (3) (2016) 1183–1196.
[25] B. Shahbazi, M. Malekzadeh, H. R. Koofigar, Robust constrained control of spacecraft formation flying, IEEE Transactions on Aerospace and Electronic Systems 53 (5) (2017) 2534–2543.
[26] A. M. Zou, K. D. Kumar, Z. G. Hou, Attitude coordination control for a group of spacecraft without velocity measurements, IEEE Transactions on Control Systems Technology 20 (5) (2012) 1160–1174.
[27] D. Ran, X. Chen, A. K. Misra, Finite time coordinated formation control for spacecraft formation flying under directed communication topology, Acta Astronautica 136 (2017) 125–136.
[28] S. Li, X. Wang, Finite-time consensus and collision avoidance control algorithms for multiple auvs, Automatica 49 (11) (2013) 3359–3367.
[29] R. Olfati-Saber, Flocking for multi-agent dynamic systems: algorithms and theory, IEEE Transactions on Automatic Control 51 (3) (2006) 401–420.
[30] P. F. Hokayem, D. M. Stipanovi, M. W. Spong, Coordination and collision avoidance for lagrangian systems with disturbances, Applied Mathematics and Computation 217 (3) (2010) 1085–1094.
[31] H. Xu, Y. Ye, Z. Yang, Underactuated spacecraft formation reconfiguration with collision avoidance, Acta Astronautica 131 (2017) 166–181.
[32] Q. Hu, H. Dong, Y. Zhang, et al, Tracking control of spacecraft formation flying with collision avoidance, Aerospace Science and Technology 42 (2015) 353–364.
[33] J. D. Biggs, L. Colley, Geometric attitude motion planning for spacecraft with pointing and actuator constraints, Journal of Guidance Control and Dynamics 39 (7) (2016) 1672–1677.
[34] H. Gui, G. Vukovich, Robust switching of modified rodrigues parameter sets for saturated global attitude control, Journal of Guidance Control and Dynamics 40 (6) (2017) 1529–1536.
[35] M. D. Shuster, Survey of attitude representations, Journal of the Astronautical Sciences 41 (4) (1993) 439–517.
[36] B. Xiao, Q. Hu, Y. Zhang, et al, Fault-tolerant tracking control of spacecraft with attitude-only measurement under actuator failures, Journal of Guidance Control and Dynamics 37 (3) (2014) 838–849.
[37] B. Xiao, S. Yin, Velocity-free fault-tolerant and uncertainty attenuation control for a class of nonlinear systems, IEEE Transactions on Industrial Electronics 63 (7) (2016) 4400–4411.
[38] H. K. Khalil, Nonlinear systems third edition, Upper Saddle River, NJ: Prentice-Hall, Inc.,2002.